buildings

Article

Analytical Assessment of the Structural Behavior of a Specific Composite Floor System at Elevated Temperatures Using a Newly Developed Hybrid Intelligence Method

Shaoyong Han [1,2], Zhun Zhu [3,*], Mina Mortazavi [4,*], Ahmed M. El-Sherbeeny [5] and Peyman Mehrabi [6]

1 School of Information Engineering and Technology, Changzhou Vocational Institute of Industry Technology, Changzhou 213164, China
2 Postdoctoral Scientific Research Workstation, Bank of Zhengzhou, Zhengzhou 450015, China
3 School of Information Engineering, Wenzhou Business College, Wenzhou 325035, China
4 School of Civil and Environmental Engineering, Faculty of Engineering and Information Technology, University of Technology Sydney (UTS), Ultimo, NSW 2007, Australia
5 Industrial Engineering Department, College of Engineering, King Saud University, P.O. Box 800, Riyadh 11421, Saudi Arabia
6 Centre for Infrastructure Engineering, Western Sydney University, Penrith, NSW 2751, Australia
* Correspondence: zhuzhun@wzbc.edu.cn (Z.Z.); mina.mortazavi@uts.edu.au (M.M.)

Abstract: The aim of this paper is to study the performance of a composite floor system at different heat stages using artificial intelligence to derive a sustainable design and to select the most critical factors for a sustainable floor system at elevated temperatures. In a composite floor system, load bearing is due to composite action between steel and concrete materials which is achieved by using shear connectors. Although shear connectors play an important role in the performance of a composite floor system by transferring shear force from the concrete to the steel profile, if the composite floor system is exposed to high temperature conditions excessive deformations may reduce the shear-bearing capacity of the composite floor system. Therefore, in this paper, the slip response of angle shear connectors is evaluated by using artificial intelligence techniques to determine the performance of a composite floor system during high temperatures. Accordingly, authenticated experimental data on monotonic loading of a composite steel-concrete floor system in different heat stages were employed for analytical assessment. Moreover, an artificial neural network was developed with a fuzzy system (ANFIS) optimized by using a genetic algorithm (GA) and particle swarm optimization (PSO), namely the ANFIS-PSO-GA (ANPG) method. In addition, the results of the ANPG method were compared with those of an extreme learning machine (ELM) method and a radial basis function network (RBFN) method. The mechanical and geometrical properties of the shear connectors and the temperatures were included in the dataset. Based on the results, although the behavior of the composite floor system was accurately predicted by the three methods, the RBFN and ANPG methods represented the most accurate values for split-tensile load and slip prediction, respectively. Based on the numerical results, since the slip response had a rational relationship with the load and geometrical parameters, it was dramatically predictable. In addition, slip response and temperature were determined as the most critical factors affecting the shear-bearing capacity of the composite floor system at elevated temperatures.

Keywords: extreme learning machine; radial basis function network; neural network; shear connector; floor system; elevated temperature; metaheuristic algorithms

check for updates

Citation: Han, S.; Zhu, Z.; Mortazavi, M.; El-Sherbeeny, A.M.; Mehrabi, P. Analytical Assessment of the Structural Behavior of a Specific Composite Floor System at Elevated Temperatures Using a Newly Developed Hybrid Intelligence Method. *Buildings* **2023**, *13*, 799. https://doi.org/10.3390/buildings13030799

Academic Editors: Carlos Humberto Martins, Alexandre Rossi and Yasin Onuralp Özkılıç

Received: 16 January 2023
Revised: 11 March 2023
Accepted: 11 March 2023
Published: 17 March 2023

1. Introduction

Fire safety is a major concern that has not been well developed in recent years. Many studies have been conducted on a range of approaches to mitigate fire-induced damage to steel and concrete members [1–3]. Some research studies have also focused on improving the safety of occupants during and after fire occurrences and on reducing the refurbishment and retrofitting costs.

Composite beams have been widely used in a variety of structures and buildings due to a number of positive features such as lower thickness, considerable span length and high stiffness [4,5]. The development of different composite beams is highly valued to mitigate some shortcomings of specific composite structures [6–8]. Steel-concrete composite beams are one of the critical components of high rise and multi-story structures, and different studies have been conducted to improve their performance [9,10]. Moreover, shear connectors (SCs) are one of the most practical elements that are extensively utilized in steel-concrete composite beams to increase shear strength and the integrated behavior of concrete and steel. There are different types of SCs such as channel, angle, stud and perfobond sections. Concrete is cast in different shapes and types such as self-consolidating [11], porous [12], high strength, lightweight and green concrete [13]. Concrete characteristics are divided into two major categories namely fresh and hardened properties. Fresh properties include the most primitive properties of concrete such as slump and workability. On the contrary, hardened properties refer to a range of critical features such as compressive strength, flexural strength, shear strength and corrosion resistance, where many attempts have been made to enhance these properties by surface protection [14,15], the inclusion of fibers and cementitious replacement powders [16].

A few studies have considered push-out tests with various loading patterns to evaluate slip and failure load in channel SCs [17]. Channel SCs have been shown to exhibit ductile performance when exposed to a series of load patterns while equipped with c-shaped connectors; however, this behavior was amplified in more extended channel SCs [18]. In another study, composite beams showed brittle behavior when channel SCs were embedded in plain concrete with no confinement [19]. In contrast, when the channel SCs were embedded in high-strength concrete, the behavior of the composite beam was ductile. In addition, more extended channel SCs demonstrated better flexibility than lower channels [19]. Bearing capacity has a direct linear relationship with length, and therefore, a C-shaped channel SC with 150 mm length has almost 60 percent higher load-carrying capacity compared to a 100 mm channel SC. In addition, failure modes are governed by concrete properties when a C-shaped channel SC is embedded in high-strength concrete [20]. Despite the inevitable slip between an I-beam and slab, this slip can be negligible with appropriate design of the shear connector. Thick channel connectors result in reducing slip and consequently increasing load capacity [21].

Angle SCs present suitable ductility but a noticeable stiffness loss [22]. Using angle shear connectors at elevated temperatures has been shown to protect strength loss by up to 50% of the initial strength [23]. Three main failure modes have occurred during tests: (1) shear connector fracture, (2) concrete crushing and (3) concrete shear plane failure. Based on experimental results, connectors' strength loss and deterioration while exposed to fire can be changed in different situations [24,25]. Several methods have been employed for data validation such as artificial neural networks, whereas extreme learning machine [21,26], genetic programming, neural network and other natural basis functional networks have been reported to be the best methods [27]. Finite element and finite strip methods have also been proven to be reliable approaches for data authentication and prediction [28–33].

The role of AI techniques has recently been highlighted in the. development of engineering goals [25,34,35]. A raw model of artificial neural networks (ANNs) can generally be developed by training and optimization techniques such as backpropagation algorithms [36]. Then, ANNs are able to solve three types of problems: (1) classification, (2) function approximation and (3) time series prediction. However, not being able to proceed with local extrema and complications in crossing plateaus of error function landscape are common defects of classic approaches [37]. Neural networks and some optimization techniques have recently been applied to solve nonlinear and sophisticated engineering problems. In some cases, the performance of an ANN can be improved by using the global search feature of classic methods such as GA and PSO [26]. As a remedy for ANN problems, a fuzzy technique has been integrated with neural networks, and other algorithms have been developed such as the artificial neuro fuzzy inference system (ANFIS) [38], which has been used for different types of applications including the prediction of experimental results with nonlinear relationships and parameter identification of the test data. Studies have shown that an ANFIS alone has some shortcomings which could be annihilated by incorporating metaheuristic algorithms [39]. Due to the relatively conventional approach of laboratory data in the steel-concrete composite sector, in addition to the studies on different SC applications to develop the structural strength of composite floor systems and raise their ductility, AI techniques can be employed to optimize and to evaluate the structural characteristics of steel-concrete composite structures [19].

In addition, several studies have used different AI techniques in comparative studies to challenge the main algorithm results and to achieve reliable outcomes [40]. In a study, the RBFN approach was selected as a secondary method to challenge the main algorithm prediction which was stochastic gradient descent. The RBFN results were also used to detect landslide susceptibility [41]. The machine learning method is another useful approach as a secondary algorithm for prediction of data and assessment of structural behavior [42]. The ELM method has been performed on data from steel-concrete composite floors at different heat stages along with an ANN and genetic programming technique. Based on the results, the ELM method accurately predicted the target outcomes and achieved superior performance indices [43]. In this study, a comparative AI assessment on data derived from a composite floor system at different heat stages was performed to predict the failure load and to obtain the most critical parameters for slip response.

In this study, we conducted a comparative AI assessment of the behavior of a composite floor system at different temperatures. In addition, three different AI methods were performed which was profoundly helpful to identify the most susceptible characteristics of the composite floor system at elevated temperatures. Predicting values for split-tensile and shear connector slip of a steel-concrete composite floor system subjected to a monotonic loading scenario at different heat stages is complicated since empirical testing is difficult and time-consuming and because the effective parameters are somehow hidden from the researchers or the outcomes of test results do not have enough consistency. Therefore, in this study, we aimed to overcome the prediction difficulties by employing an integrating neural network and fuzzy system with a multi-hybrid metaheuristic technique, called the ANPG method. The main algorithm was a hybrid AI technique carried out to predict the shear response in angle shear connectors simultaneously with an investigation of the effect of various inputs on the structural performance of a composite floor system at elevated temperatures. For this purpose, we developed the ANPG algorithm by using a hybrid metaheuristic (combination of PSO-GA) technique which was based on a neuro-fuzzy algorithm (ANFIS) due to the diverse nature of the employed data and its ability to predict the shear behavior of composite systems at high temperatures. Accordingly, some validated data from Davoodnabi et al. [23] were derived from a previous laboratory research study to delineate the shear behavior of the angle shear connectors at different temperatures. In soft computing methods, the above-mentioned methods can provide a compact solution for multi-variable method drawbacks since knowledge of the internal system is not necessary. Two proven and effective artificial intelligence algorithms, i.e., the RBFN and ELM methods, were also employed to verify and to compare the obtained results. In addition, the affect of different parameters on the shear-bearing capacity of the composite floor system were evaluated and the parameters that were the most critical factors were selected.

2. Materials and Methods

For this research, the database was obtained from the study by Davoodnabi et al. [23] regarding a monotonic push-out test on SCs at elevated temperatures to achieve reliable structural behavior of a composite system at high temperatures. The aforementioned shear connectors are shown in Figure 1.

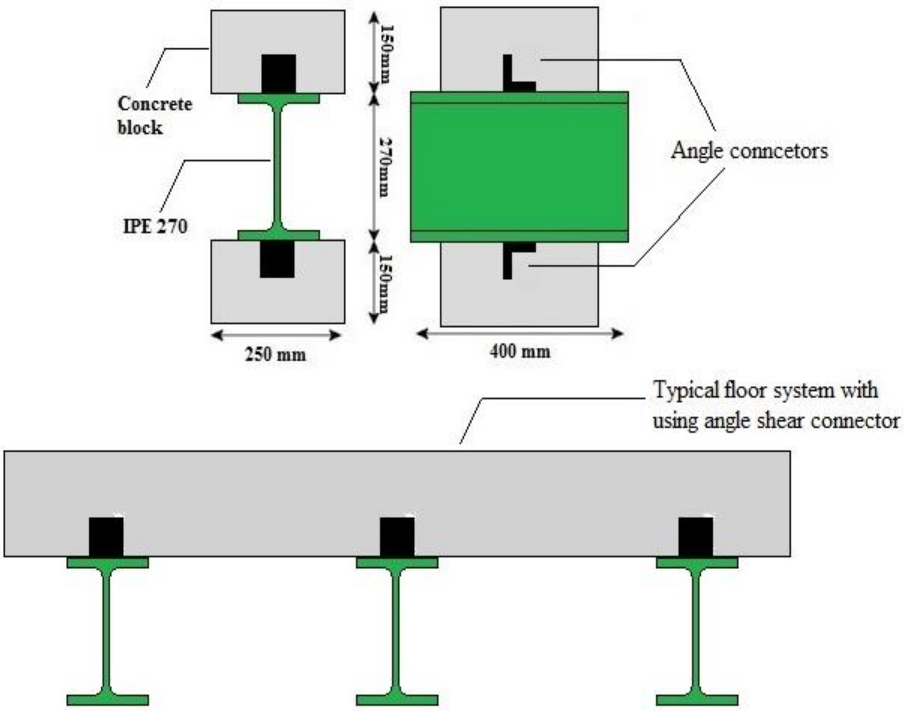

Figure 1. Composite floor system and shear connectors.

2.1. Statistical Data of Samples

In this study, the dataset was the information of experiments that eventually consisted of 584 test results (the specifications of the dataset are shown in Appendix A). The statistical properties of the whole dataset and input variables are indicated in Table 1.

Table 1. Details of input variables.

Inputs	Variables	Min	Max	Mean Value	Std
Input 1	Slip (mm)	0.00	73.70	22.87	39.2
Input 2	Length (mm)	30.0	50.0	40.0	10.0
Input 3	Thickness (mm)	5.0	7.0	6.0	0.8
Input 4	Height (mm)	65.0	100.0	80.4	14.8
Input 5	Temperature (°C)	25.0	850.0	568.2	311.9
Input 6	Load (kN)	0.00	126.7	36.8	27.6
Outputs					
Output 1	Slip (mm)	0.00	73.70	22.87	39.2
Output 2	Load (kN)	0.00	126.7	36.8	27.6

As shown in Table 1, the concrete's compressive strength along with the steel properties remained at constant values with no involvement in the dataset. The database was set for variables such as the height, length and thickness of the shear connectors, which directly affect the split-tensile capacity of the composite floor system, especially at elevated temperatures. Load and slip could be replaced by each other in the placement order either as an input or an output.

2.2. Analytical Assessment

Recently, some research studies have been conducted on the performance of welded built-up steel members using AI techniques [25]. The following sections describe the architecture and some background of the employed algorithms in the current study.

2.2.1. ANFIS Algorithm and Architecture

In an adaptive network (AN), nodes are directly connected by links, and every node acts in a defined performance on its receiving signals to produce a single node output; therefore, this procedure is made up of a multi-layer feed-forward system [34]. Notably, the configuration of an AN acts as a static node function on its receiving signals to produce a single node output, and every node performance is a parameterized function with changeable parameters. With any alteration of these parameters, the node functions are altered such as the overall behavior of the AN, Figure 2. In a fuzzy inference system (FIS), membership function parameters are tuned by a specific technique. Indeed, an ANFIS is utilized to delineate the optimal amounts of equivalent FIS parameters through a learning algorithm [44]. Across the training session(s), parameter optimization is performed in a way that the error between actual output and target decreases. A hybrid algorithm is utilized for the optimization that is a combination of gradient descent and the least square estimate method. The optimized parameters are called premise parameters that specify the shape of the membership functions (MFs). To minimize the error measure, each optimization routine could be used after the MFs are generated. The parameter set of the AN permits the fuzzy systems to learn from the modeling data.

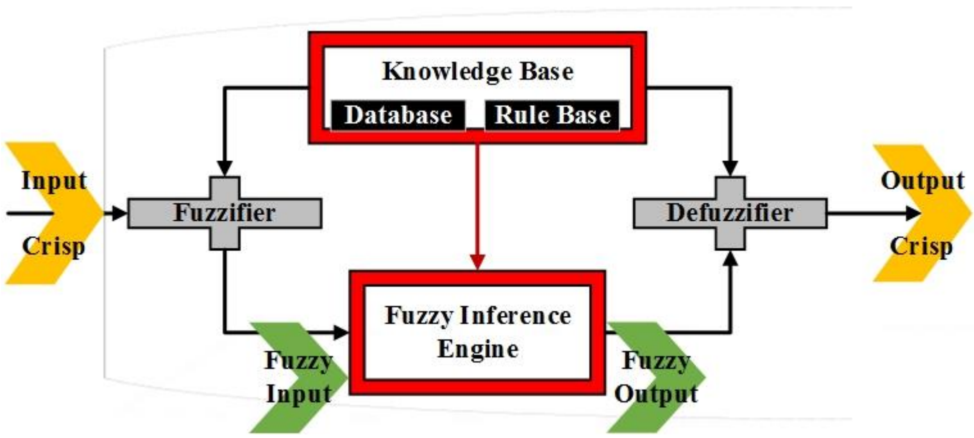

Figure 2. Flowchart of the ANFIS network concept.

The ANFIS network has five layers called the fuzzy layer, normalized layer, product layer, total output layer and de-fuzzy layer, as shown in Figure 3 [45]. During this technique, a threshold value between the output and the actual value is set and the following parameters are obtained by the least-squares model, while an error for all data is also received. If the threshold value exceeds the deliberated threshold, using the gradient descent method the premise parameters are updated. This continues until the error turns out to be less than the threshold. Because the parameters are simultaneously obtained by using two algorithms (the decent gradient and least-squares algorithms), the utilized algorithm during this procedure is called a hybrid algorithm.

2.2.2. Particle Swarm Optimization (PSO)

The PSO algorithm is another member of the swarm intelligence algorithms initially generated by Kennedy and Eberhart [46] while sharing many aspects with evolutionary computation models such as GA. Similar to other population-based intelligence models, PSO needs an initial population of random resolutions. The search for optimal values is gained by updating the generations without evolution operators such as mutation and crossover. The potential decisions are generally called particles in PSO, flying through the resolution space by following their own experiences and the current optimal particles. Thus, the performance of PSO is comparable with GA and may be regarded as an alternative approach for GA. Figure 4 indicates the systematic sequences of the PSO algorithm.

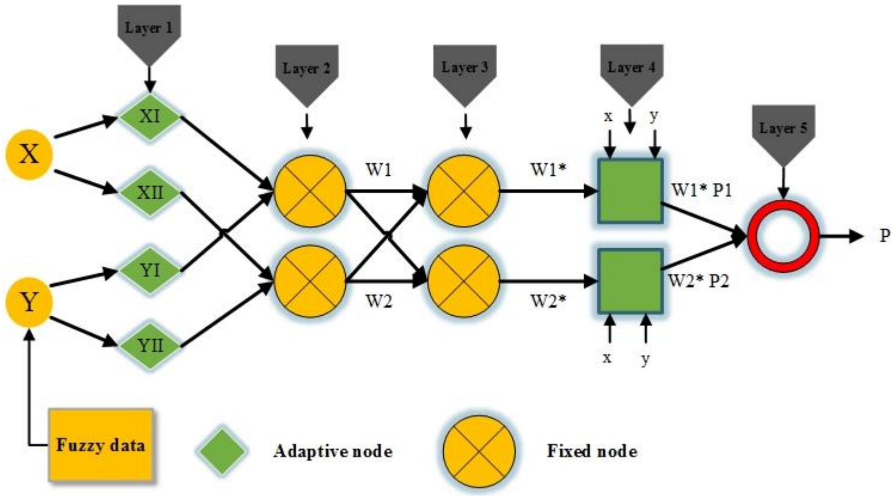

Figure 3. The underlying architecture of the ANFIS.

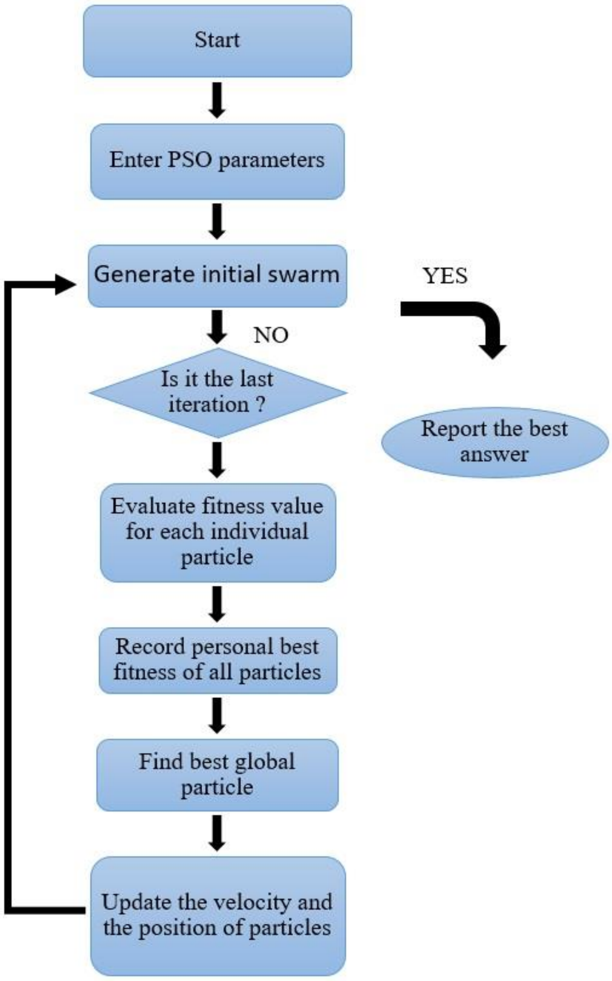

Figure 4. Flowchart of sequential steps of the PSO algorithm.

2.2.3. Genetic Algorithm (GA)

Holland (1992) [47] introduced the GA based on the extended evolution theory of Darwin that was developed by Goldberg and Holland (1988) [48]. As a member of the larger group of evolutionary algorithms (EAs), the GA is a metaheuristic algorithm based on the principles of biological evolution in nature. After many evolutions, the best individual is obtained. Compared with other optimizing methods, the GA includes good robustness and convergence. With the same accuracy of calculation, the GA takes the least time to find an optimal resolution [49]. Figure 5 represents the step-by-step platform of the GA algorithm.

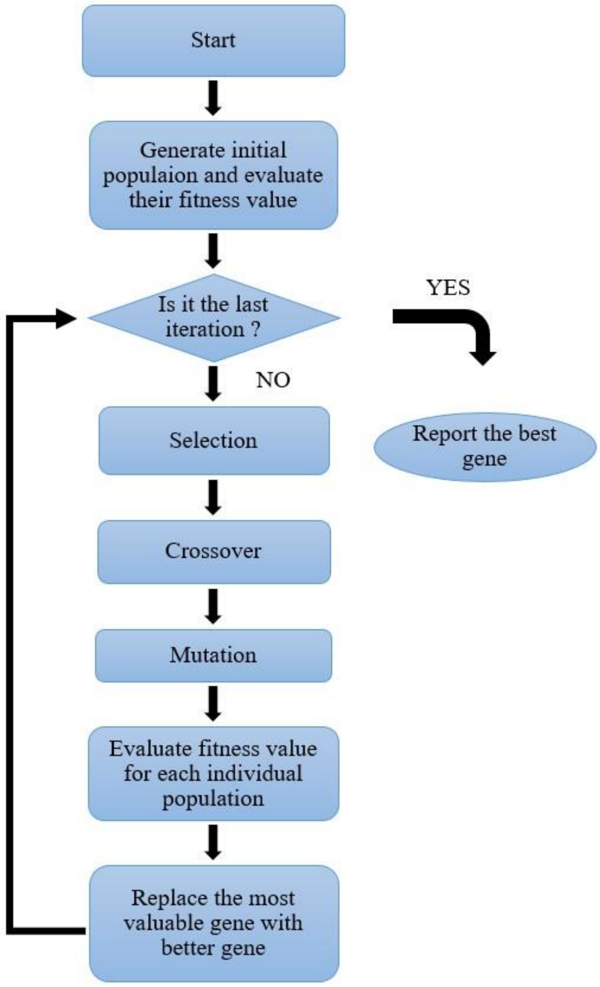

Figure 5. Flowchart of the sequential steps of the GA algorithm.

2.2.4. Hybrid ANPG Architecture

For the first time, a hybridized ANFIS using PSO and GA techniques was applied to solve a composite floor system problem. The combination of the sequential PSO-GA and ANFIS is depicted in Figure 6. In order to identify the best weights and to select suitable functions, the ANPG method was performed several times to predict one specific outcome with a variety of input scenarios. First, in PSO, swarm is initiated by a group of random resolutions as a particle, while showing the particle's position. Then, the specific velocity is identified, the transmitting function is triggered, and the GA procedure initiates to optimize the final problem space. Finally, a particular velocity is gained for any *i*th particle in every cycle by using Equation (1) where w represents the inertia weight.

$$v_i(t+1) = wv_i(t) + c_1\phi_1(p_i(t) - x_i(t)) + c_2\phi_2(p_i(t) - x_i(t)) \tag{1}$$

c_1 and c_2 represent the positive acceleration coefficients. $\vec{\phi}_1$ and $\vec{\phi}_2$ show uniformly distributed random vectors [0, 1], in which a random value is tried for each dimension. $\vec{v}_i$ limited to $\left[-\vec{v}_{\max}, \vec{v}_{\max}\right]$ series is reliant on the problem. In some cases, the velocity exceeds the mentioned curb and is rearranged within its suitable limits. Based on their velocities, every particle alters its position based on the following Equation (2):

$$s(t+1) = s(t) + v(t+1) \tag{2}$$

Based on $\vec{v}_i$ and $\vec{s}_i$, the particle population tends to cluster around the best number.

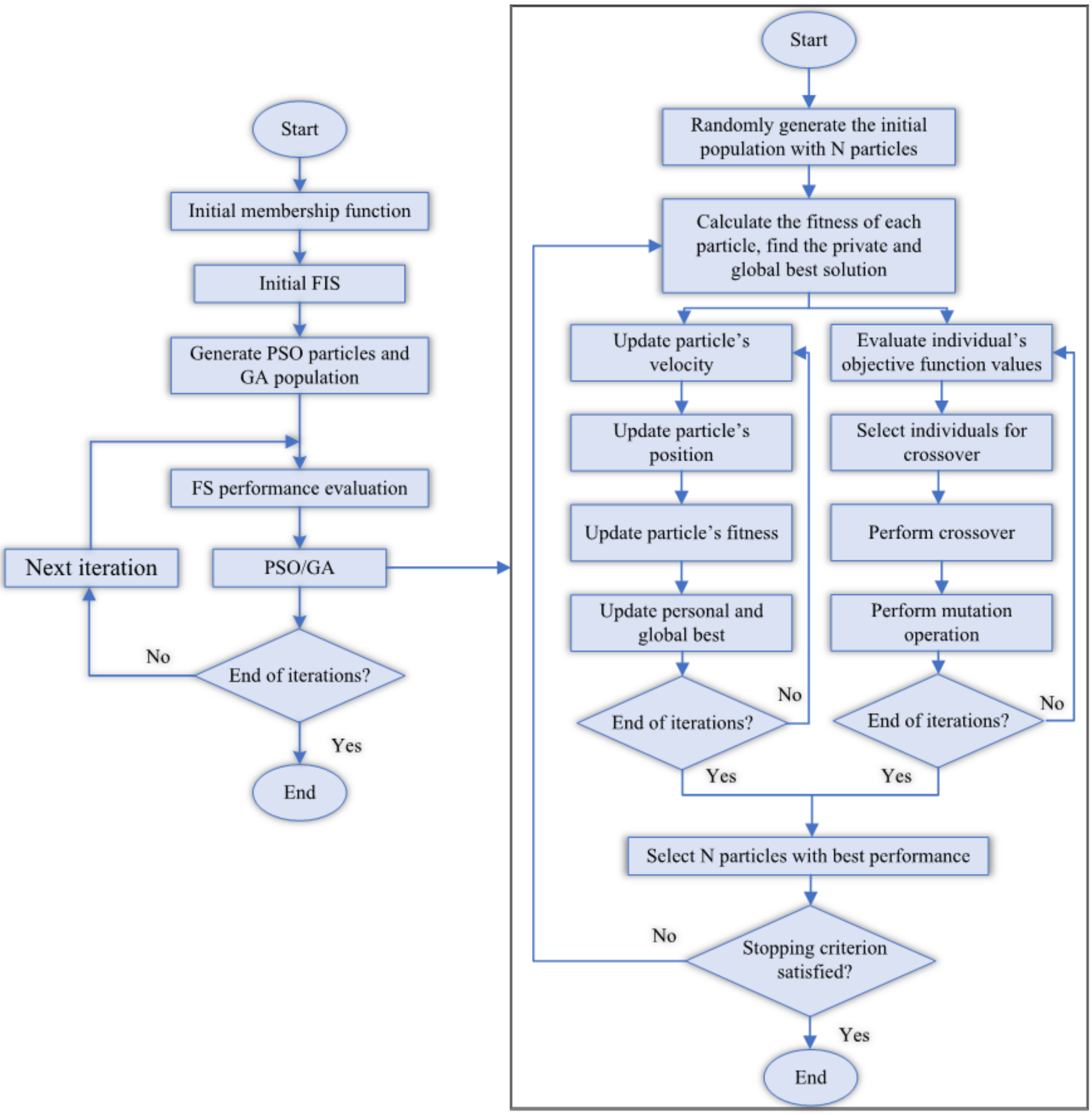

Figure 6. The sequential combination of the hybrid ANPG algorithm.

The ANPG hybrid method operates in regard to random population generation and is based on avian mass flight behavior modeling and simulation of fish mass movement. A global minimization method can deal with questions whose answers are a point or surface in n-dimensional space. A random population is assumed in this space, and an elementary velocity is defined for it and between the particles to the communication channels. The particles move through the response space, and the outcomes are computed on a "merit basis" after each time interval. Then, particles speed up toward the particles of higher competence that are in matching communication groups. Although each method is performed satisfactorily in a range of problems, it demonstrates pronounced capability in resolving continuous problems in optimization. The GA, by using evolutionary biology methods, tries to find the optimum formula for predicting or pattern matching. The GA could be an effective choice for regression-based prediction techniques, while its modeling is a programming technique based on genetic evolution to problem resolutions. The solved problem possesses inputs converted into solutions through a patterned process of genetic evolution. Afterward, by using the fitness function, the solutions are verified as candidates. The ANPG algorithm terminates in case the condition of problem exit is arranged. Generally, it is an iteration-based algorithm in which most of its parts are randomly selected.

2.2.5. Extreme Learning Machine (ELM)

As a single-layer learning tool, the ELM method was introduced which is similar to a feed-forward neural network [50]. In the ELM method, the output weights are analytically determined while the weights of input are defined randomly. The superiority of the ELM method is its extremely fast ability to find target weights. Additionally, without exterior interference, the ELM method is able to determine all the network parameters. In the case of prediction and characteristic estimation for concrete products, the ELM method is efficient and reliable [51] and because of these benefits it has gained high popularity and applicability.

2.2.6. Radial Basis Function Network (RBFN) Method

Generally, in each RBFN architecture, a set of D-dimensional radial activation functions estimate the input function $f_{(x)}$. The architecture consists of the D neuron input layer, the P neuron output layer and the M neuron hidden layer. The biases at each output neuron and adjustable weights between the hidden and output layers are shown in Figure 7 [52,53]. The system is represented by the nth input vector, and as described in Equation (3), the approximation function $f_{(x)}$ can be represented as a linear combination of radial basis functions in which the output of the kth network consists of the sum of weighted hidden layer neurons plus the bias [41]:

$$\hat{f}(X) = wh(X) + w, k = 1, 2, \ldots, P \tag{3}$$

where:

w_{kj} = weight of the jth basis function and kth output;
h_j (X^n) = output of jth hidden neuron for the input vector (x^n);
$w_{(k0)}$ = bias term at kth output neuron.

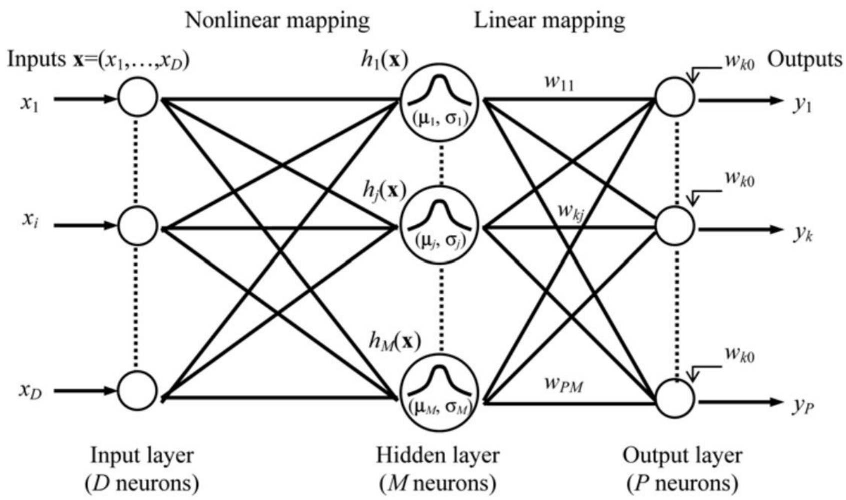

Figure 7. The architecture of the RBF network.

2.2.7. Performance Evaluation

Models of all the developed methods were evaluated by using evaluation criteria namely, root mean squared error (RMSE), determination coefficient (R^2) and Pearson correlation coefficient (r) as follows:

$$RMSE = \sqrt{\frac{\sum_{i=1}^{n}(P_i - O_i)^2}{n}} \tag{4}$$

$$\mathrm{r} = \frac{\mathrm{n}\left(\sum_{i=1}^{n} \mathrm{O_i} \cdot \mathrm{P_i}\right) - \left(\sum_{i=1}^{n} \mathrm{O_i}\right) \cdot \left(\sum_{i=1}^{n} \mathrm{P_i}\right)}{\sqrt{\left(\mathrm{n}\sum_{i=1}^{n} \mathrm{O_i^2} - \left(\sum_{i=1}^{n} \mathrm{O_i}\right)^2\right) \cdot \left(\mathrm{n}\sum_{i=1}^{n} \mathrm{P_i}^2 - \left(\sum_{i=1}^{n} \mathrm{P_i}\right)^2\right)}} \tag{5}$$

$$\mathrm{R}^2 = \frac{\left[\sum_{i=1}^{n} \left(\mathrm{O_i} - \overline{\mathrm{O_i}}\right) \cdot \left(\mathrm{P_i} - \overline{\mathrm{P_i}}\right)\right]^2}{\sum_{i=1}^{n} \left(\mathrm{O_i} - \overline{\mathrm{O_i}}\right) \cdot \sum_{i=1}^{n} \left(\mathrm{P_i} - \overline{\mathrm{P_i}}\right)} \tag{6}$$

where P_i and O_i are the predicted and observed variables, and n is the total number of considered data. Alternatively, MATLAB (2019) was used to compare the code performance of the ANPG, RBFN and ELM methods in one computer system with no external compiler or toolbox implementation.

3. Results

In this study, the employed algorithms (the ANPG, RBFN and ELM methods) were separately tuned. To optimize the coefficients of specific parameters for each algorithm, the other parameters were considered to remain constant. By changing the coefficient value, the best value was determined and used for different parameters. Therefore, all the algorithms were repeatedly used and revised to develop the algorithms, as explained below.

3.1. ANFIS-PSO-GA (ANPG) Method

The parameters of the ANPG method were adjusted and are summarized in Table 2. The inputs of the dataset were initially defined and predicted, while the predition values of split-tensile load and slip were obtained separately in different analyses (Table 2). The results of the regression and comparative graphs are shown in Figures 8 and 9, respectively. As shown in Figure 8 and Table 3, the ANPG method is more successful for predicting values of slip than for predicting tensile load, which could be due to the properties of this type of NN or simply to the output being more predictable. In addition, the test results of slip and load prediction demonstrate good consistency with the training results, indicating the reliability of this method for predicting complex and nonlinear test results. Despite the acceptability of the outputs of the other employed ELM method, the inconsistent test and training results reduced the reliability of the output(s).

Table 2. Parameter characteristics used for the ANPG method.

FIS Clusters	Population Size	PSO-Iterations	GA-Sub-Iteration	MAX-Iteration	Inertia Weight	Damping Ratio	Learning Coefficient		Conducted Fuzzy Function
							Personal	Global	
10	90	50	45	150	1.00	0.988	1	2	bell-shaped

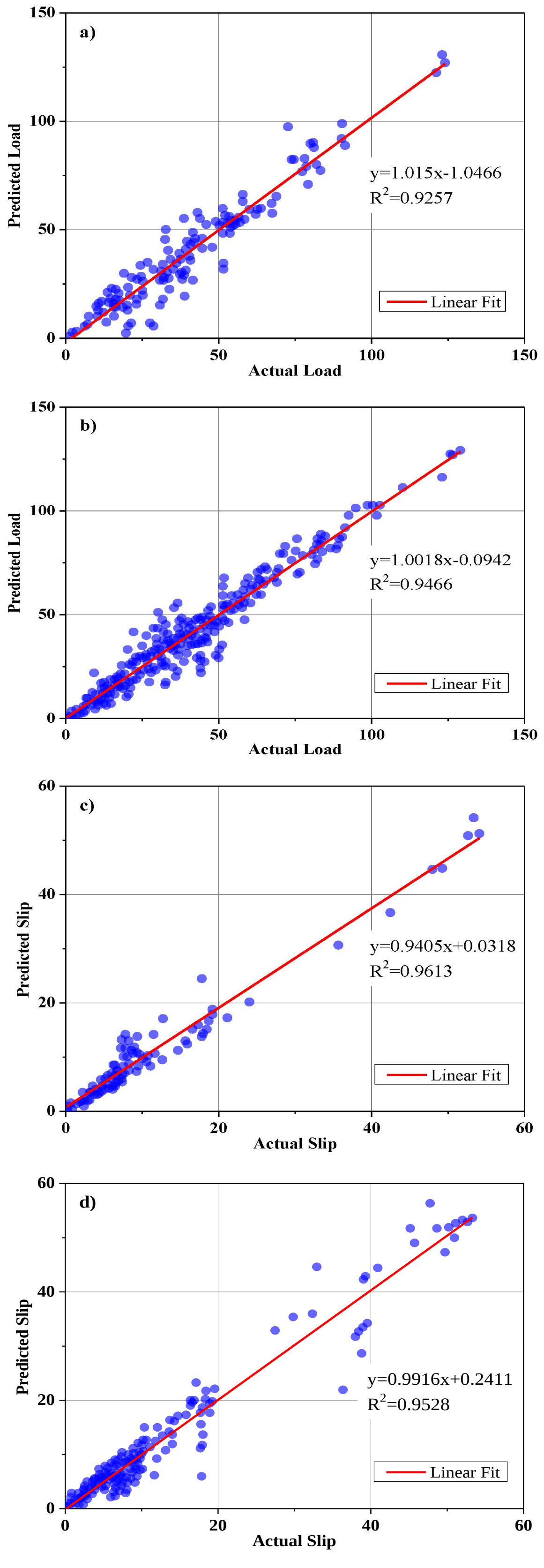

Figure 8. ANPG vs. experimental results regression for: (**a**) Ultimate shear load test phase; (**b**) ultimate shear load training phase; (**c**) slip test phase; (**d**) slip training phase.

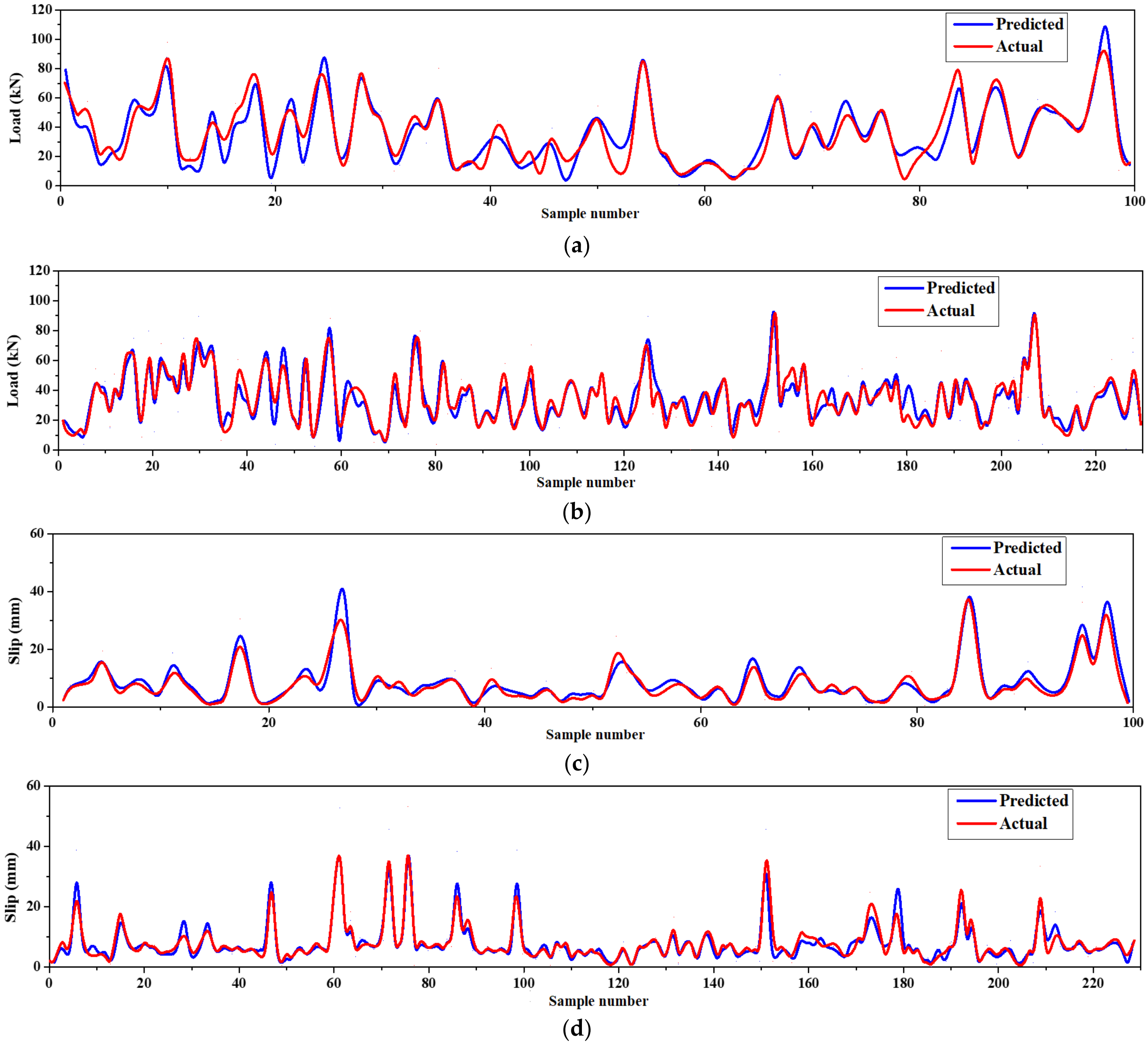

Figure 9. ANPG vs. experimental diagram for: (**a**) Ultimate shear load test phase; (**b**) ultimate shear load training phase; (**c**) slip test phase; (**d**) slip training phase.

Table 3. Output and input database.

		Test	Train
Split-tensile load prediction	Std *	3.869	3.1884
	e_{mean}	−0.014	−0.081
	R^2	0.925	0.946
	r	0.962	0.973
	RMSE	3.869	4.868
		Test	**Train**
Slip prediction	Std *	0.954	1.136
	e_{mean}	−0.012	−0.049
	R^2	0.961	0.953
	r	0.980	0.976
	RMSE	0.962	1.736

* Std, standard deviation.

For the tensile load, the standard deviation of the two test and training phases is 18%, and the standard deviation is 16% for slip value outputs, indicating less error concentration in the first output than the second output, Figure 10.

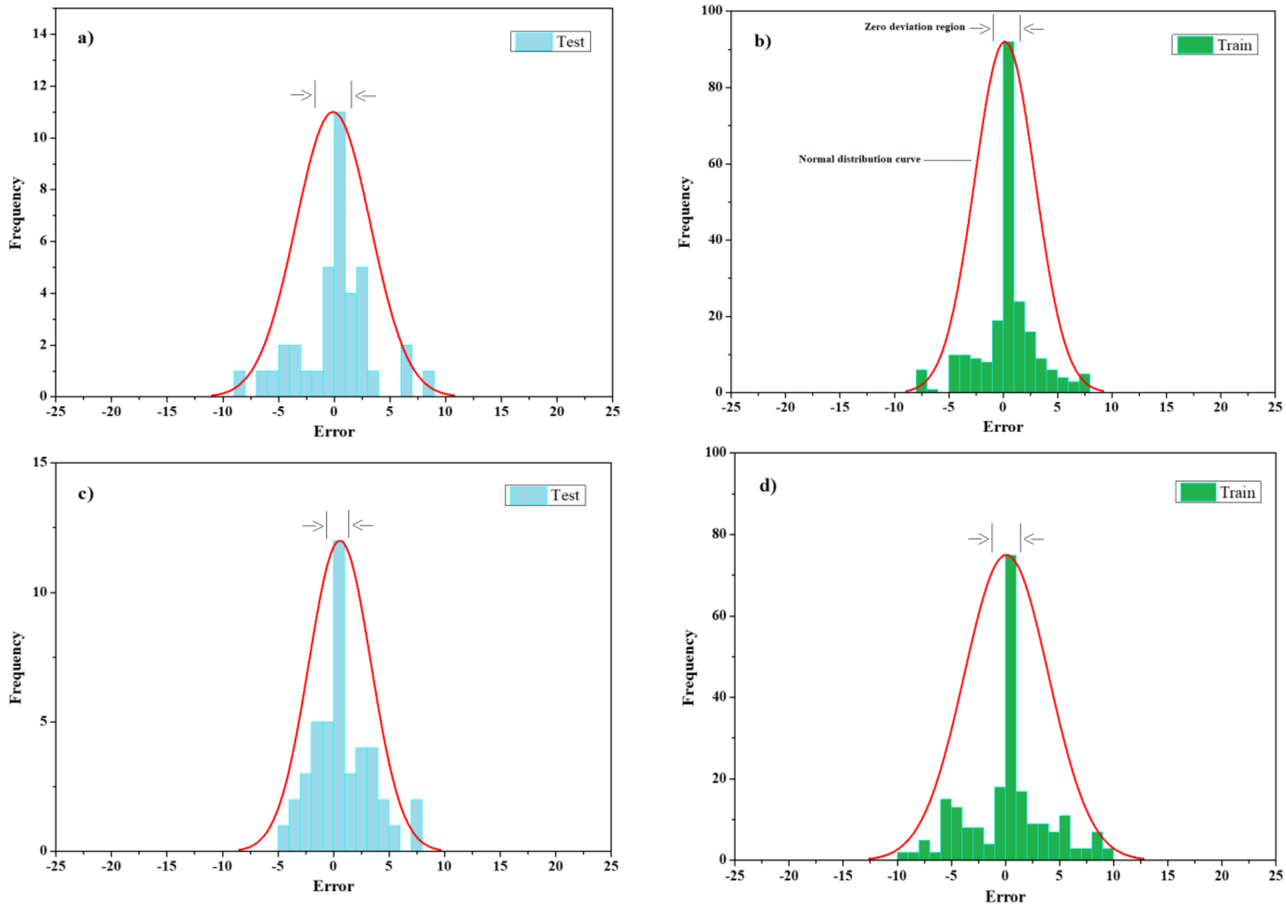

Figure 10. ANPG vs. experimental results regression for: (**a**) Split-tensile load test phase; (**b**) split-tensile load training phase; (**c**) slip test phase; (**d**) slip training phase.

3.2. RBFN

Table 4 shows the settings used for the combination of a hybrid grid. The results of the RBFN method are presented in Table 5 and Figures 11 and 12. In this method, the results for the lateral load output were much better than the compressive strength. In addition, the test and training phase results for the first output were very similar.

Table 4. The parameter characteristics used for the RBFN method.

FIS Clusters	Population Size	MAX-Iteration	Cross over Percentage	Mutation Percentage	Mutation Rate	Selection Pressure
10	180	200	1.00	0.5	0.1	8

Table 5. Analytical prediction results through the RBFN method.

		Test	Train
Split-tensile load prediction	Std *	3.950	3.003
	e_{mean}	−0.119	2.75×10^{-5}
	R^2	0.946	0.959
	r	0.972	0.979
	RMSE	3.949	4.585
		Test	**Train**
Slip prediction	Std *	1.556	1.330
	e_{mean}	−0.155	−0.036
	R^2	0.906	0.948
	r	0.952	0.973
	RMSE	1.562	2.033

* Std, standard deviation.

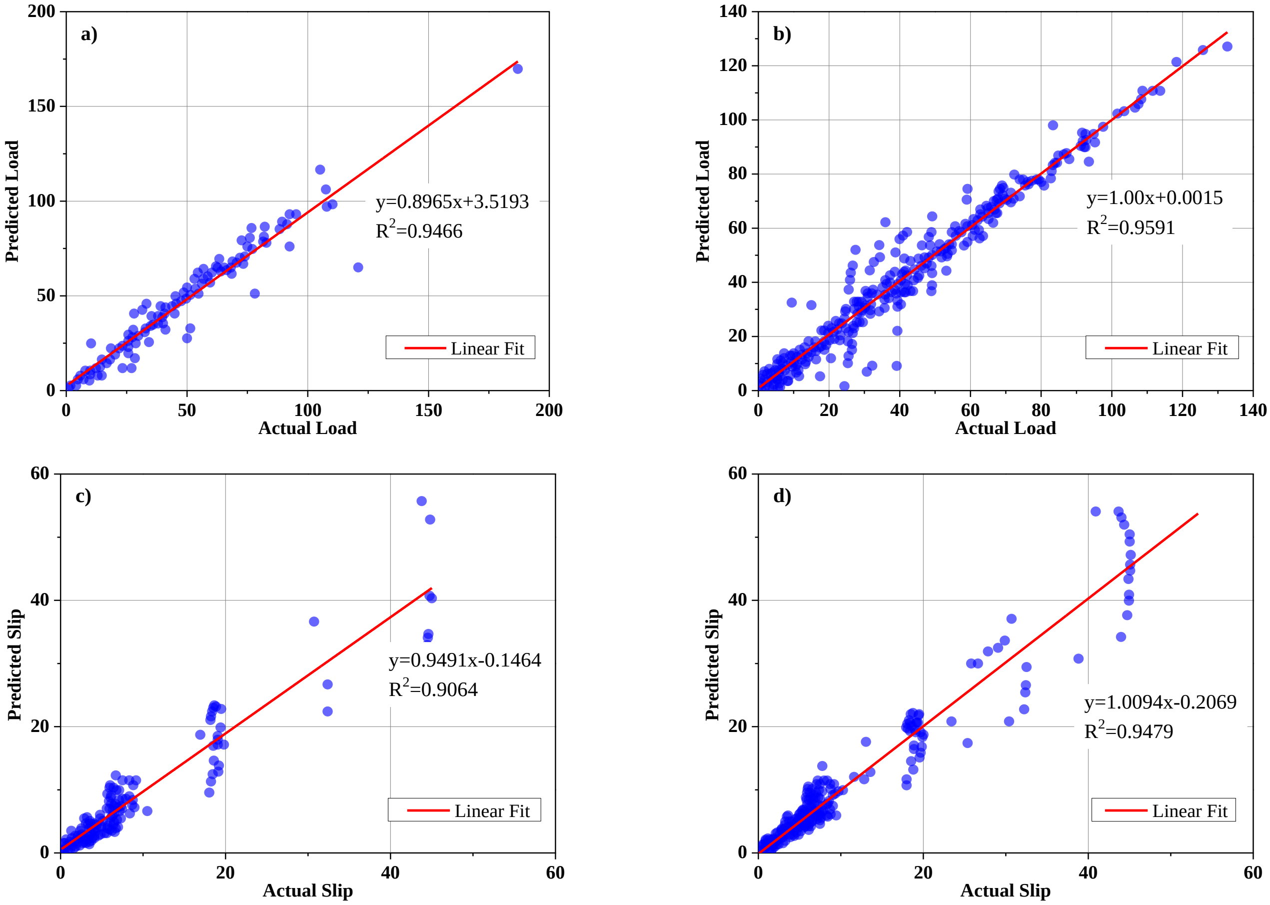

Figure 11. RBFN vs. experimental results regression for: (**a**) Ultimate shear load test phase; (**b**) ultimate shear load training phase; (**c**) slip test phase; (**d**) slip training phase.

The results of this neural network approximation for the tensile e-load value output indicated more concentration at the boundary. In particular, during the training phase, the reliable evaluation criteria results are approximate. Another point to note from the graphs in Figure 12 is the relatively low error for tensile-load data below 5 MPa for both the training and test phases and relatively high error for data above 20 MPa, especially during the training phase (Figure 12). Furthermore, slip value outputs indicate higher irregularities above 10 mm. The standard deviation of the test and training phases for the tensile load is 24% and the standard deviation is 15% for slip value outputs, indicating a better concentration of errors in slip output than load output (Figure 13).

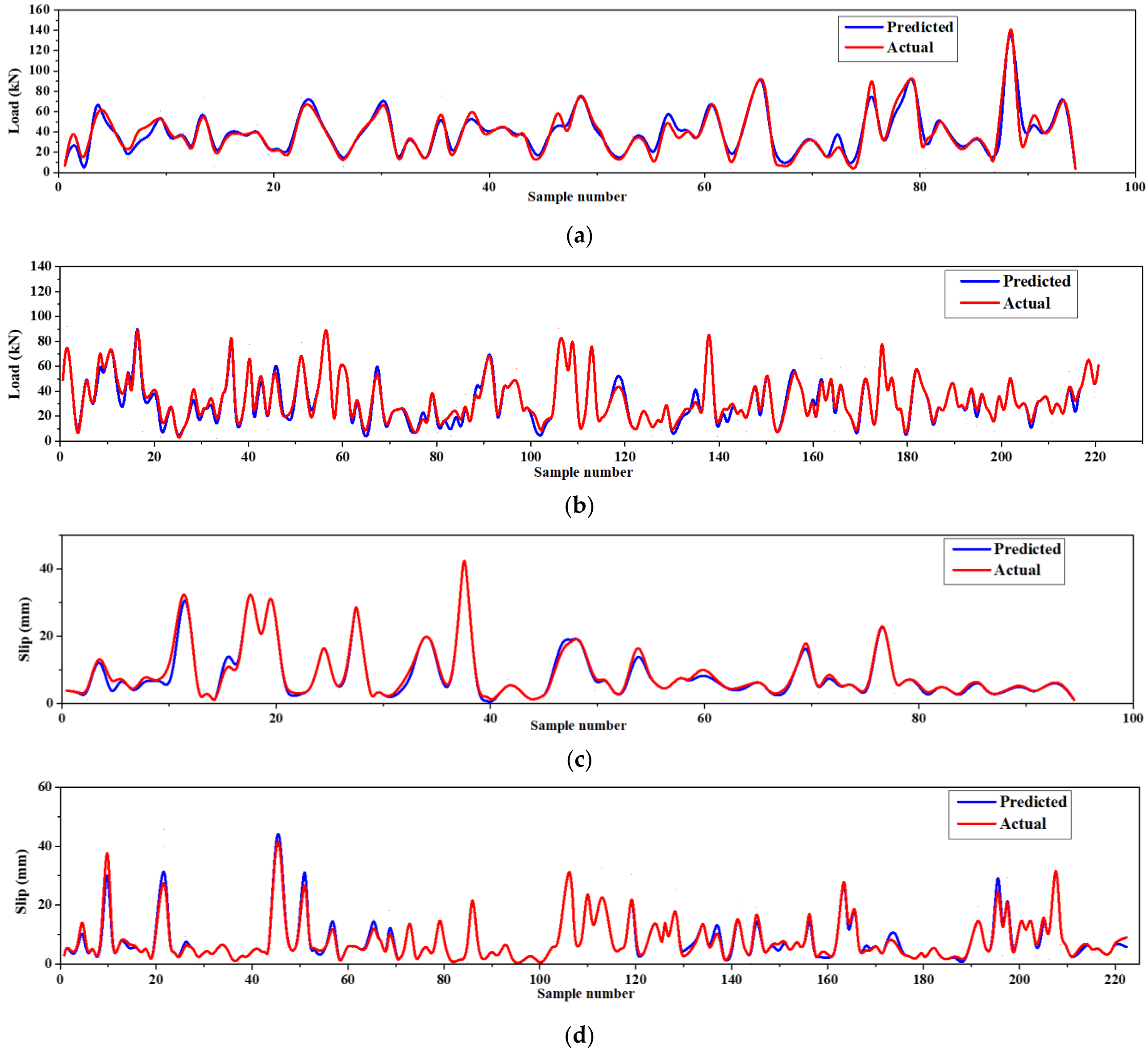

Figure 12. RBFN vs. experimental diagram for: (**a**) Split-tensile load test phase; (**b**) split-tensile load training phase; (**c**) slip test phase; (**d**) slip training phase.

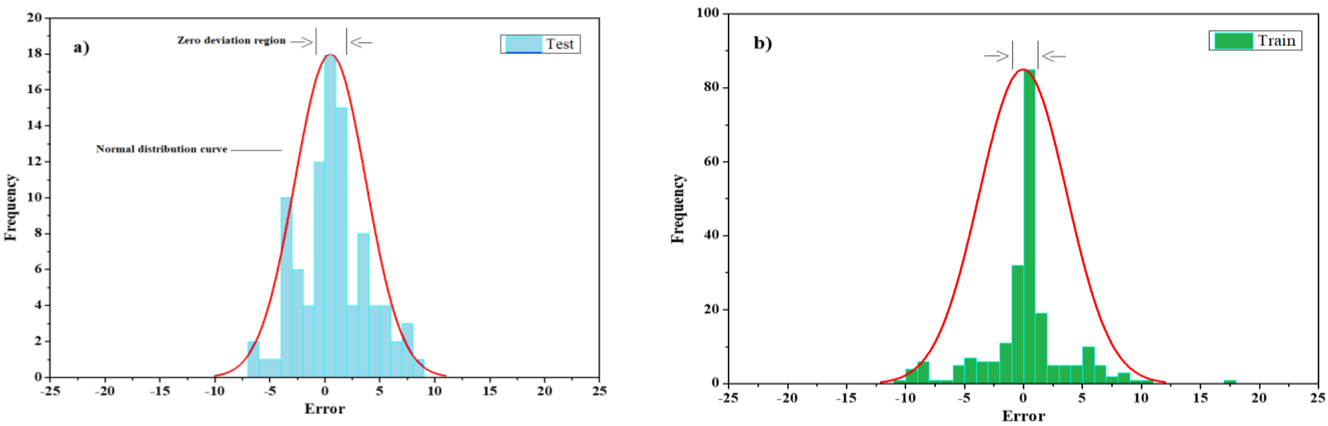

Figure 13. *Cont.*

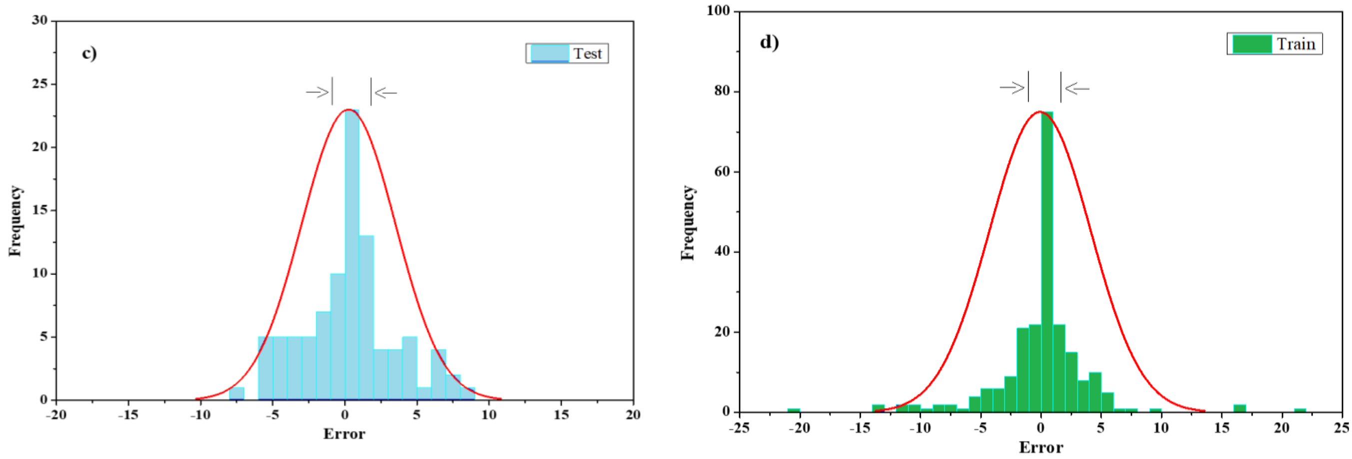

Figure 13. RBFN error histogram for: (**a**) Split-tensile load test phase; (**b**) split-tensile load training phase; (**c**) slip test phase; (**d**) slip training phase.

3.3. ELM Method

The last neural network is the ELM method and the settings and are summarized in Table 6. The results are also acceptable for both outputs, as shown in Figures 14 and 15. However, by comparing the load output evaluation criteria to those of the slip value outputs and by comparing the test and training results, the load outputs show more consistency. At the same time, it is different for other products, as shown in Table 7.

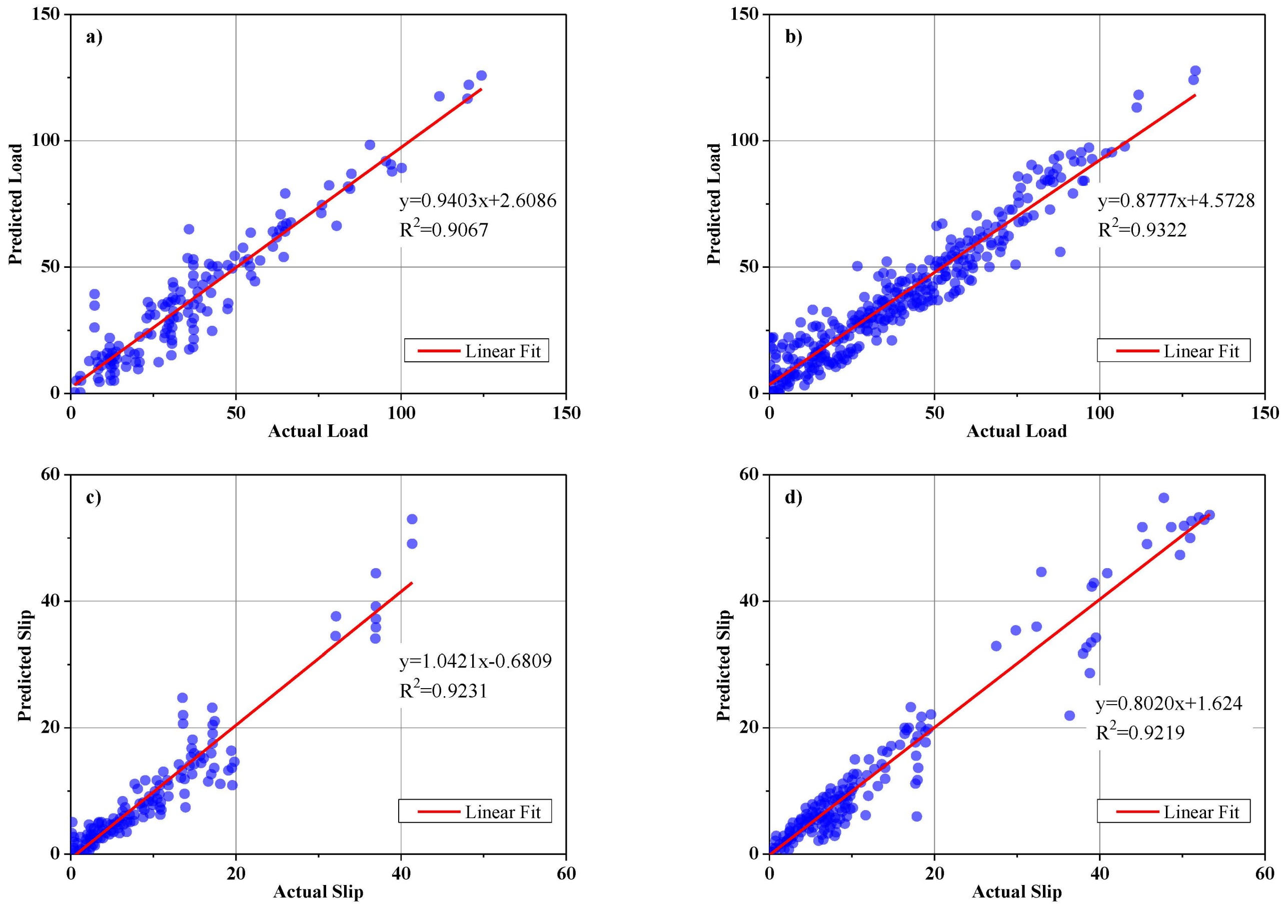

Figure 14. ELM vs. experimental results regression for: (**a**) Ultimate shear load test phase; (**b**) ultimate shear load training phase; (**c**) slip test phase; (**d**) slip training phase.

Table 6. The parameter characteristics used for the ELM method.

FIS Clusters	Regression	Hidden Neurons	Activation Function
1.0	0.008	845	Hard Limited

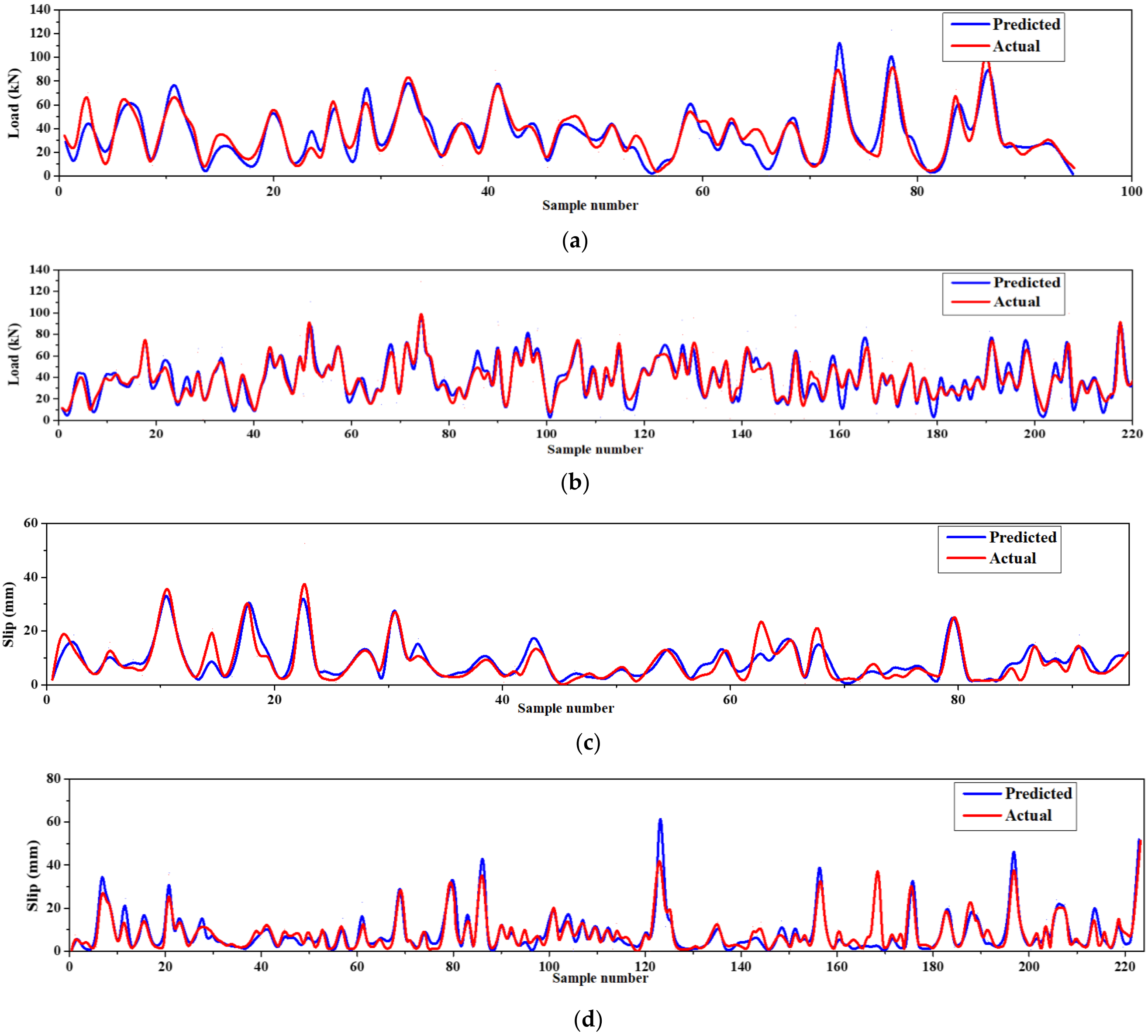

Figure 15. ELM vs. experimental diagram for: (**a**) Split-tensile load test phase; (**b**) split-tensile load training phase; (**c**) slip test phase; (**d**) slip training phase.

Regarding the standard deviation and error histogram in Figure 16, errors have a greater focus on slip value outputs which make the outputs more reliable. The tensile-load outputs presented are probably good results; however, due to the lack of focus on the errors of the center axis, an unprecedented response could be high with unacceptable errors.

Table 7. Analytical prediction results through the ELM algorithm.

		Test	Train
Split-tensile load prediction	Std *	4.341	3.949
	e_{mean}	0.128	0.022
	R^2	0.906	0.932
	r	0.9522	0.965
	RMSE	4.339	6.030
		Test	**Train**
Slip prediction	Std *	1.454	1.851
	e_{mean}	−0.086	0.044
	R^2	0.923	0.922
	r	0.961	0.960
	RMSE	1.455	2.827

* Std, standard deviation.

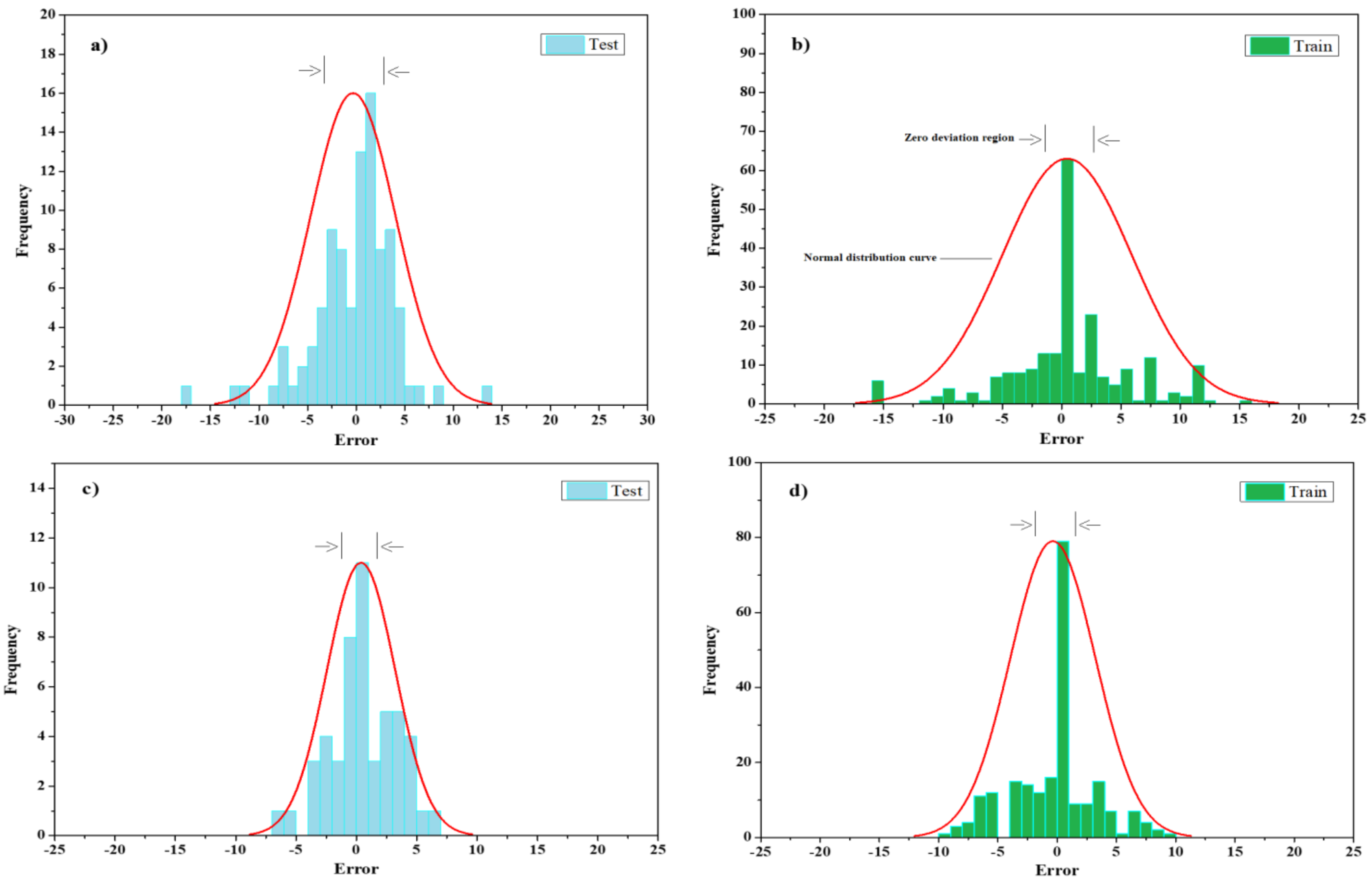

Figure 16. ELM error histogram for: (**a**) Split-tensile load test phase; (**b**) split-tensile load training phase; (**c**) slip test phase; (**d**) slip training phase.

4. Discussion

To define the inputs of RMSE, R^2 and r, an ANFIS was individually trained for every input. The effect of every input on the output could be delineated based on the determined analytical parameters for any input. Inputs with the smallest training RMSE had the most effect or relevance to the output. To identify the overfitting between test data and training, RMSE testing was applied. If the testing RMSE is very high, the regression of data is not beneficial. According to the RMSE training, the optimum combination is PSO and the GA with an ANFIS, with the most substantial accuracy on the output evaluation parameters. By examining the results of all methods, it is concluded that both split-tensile load and slip value outputs indicate a likely predictable trend due to the described inputs and useful employed NNs. A comparison of the best results for each method is shown in Figure 17, where the RBFN prediction is stronger compared to the others with R^2 (test) = 0.9466, R^2 (train) = 0.9591; r (test) = 0.973, r (train) = 0.973; and RMSE (test) = 3.949, RMSE (train) = 4.585. By evaluating the test phase error histograms shown in Figures 10, 13 and 16, due to the minor error interval in the ANPG method, the three graphs show reasonable concentration around the center, and the chance of obtaining a high error response is relatively low compared to the other methods. From the normal distribution point of view in each rectangular histogram of error, 68% of the data are within one time of the standard deviation of the mean value, 95% of the data are within two times of the standard deviation, and 99.7% of the data are within three times of the standard deviation [54–56]. Based on the results and discussion, all of the represented histograms in this paper are in agreement with the mentioned fact. Nevertheless, the charts (load error histograms) are consistent with the normal distribution paradigm, but according to Tables 3–5, different standard deviations and mean values lead to different shapes of the bell curves of load charts compared to the slip charts.

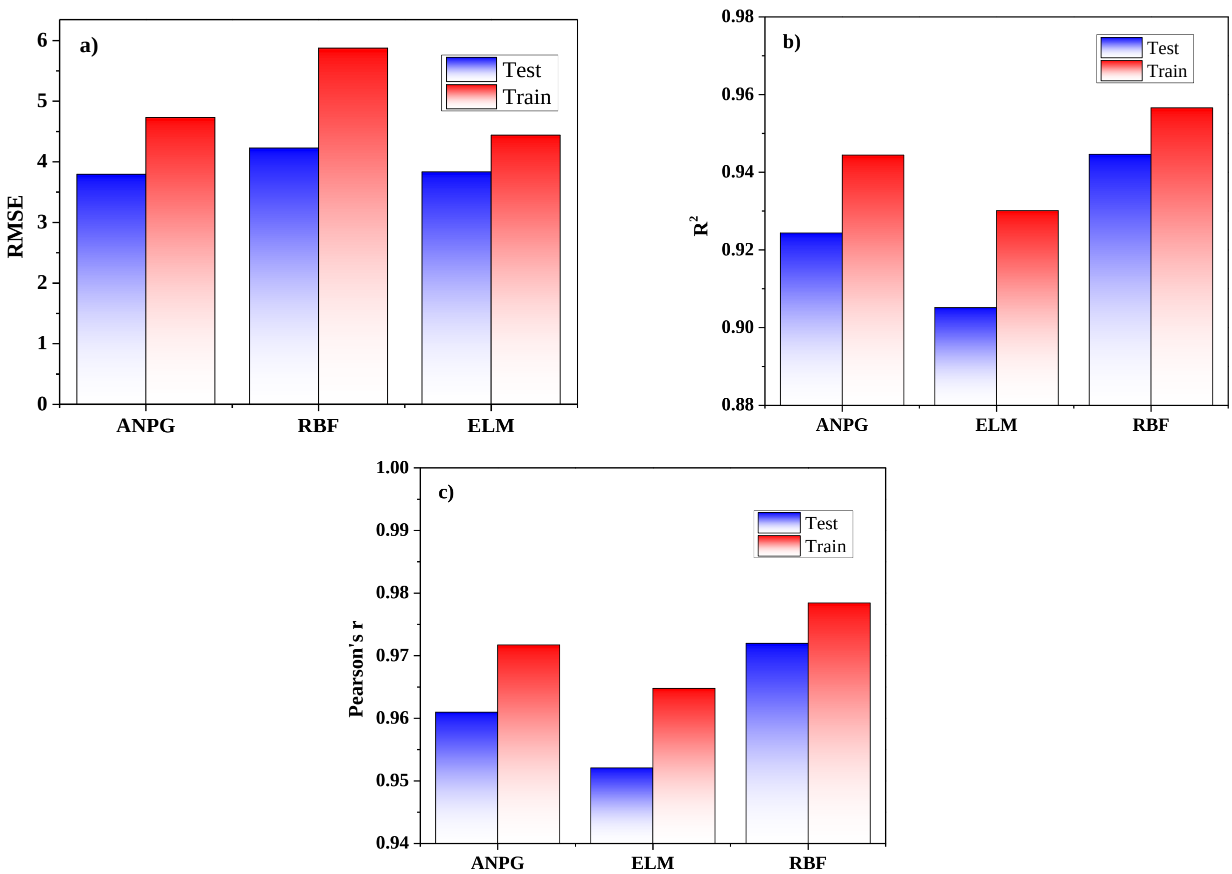

Figure 17. The comparison of performed algorithm results of split-tensile load based on: (**a**) RMSE; (**b**) R^2; (**c**) r.

For slip value output, the ANPG method also provides the best result, as shown in Figure 18. The evaluation of the test phase for the ANPG method is R^2 (test) = 0.961, R^2 (train) = 0.952; r (test) = 0.980, r (train) = 0.976; and RMSE (test) = 0.962, RMSE (train) = 1.735. Thus, in the test phase, the result presented by the ANPG method is more acceptable.

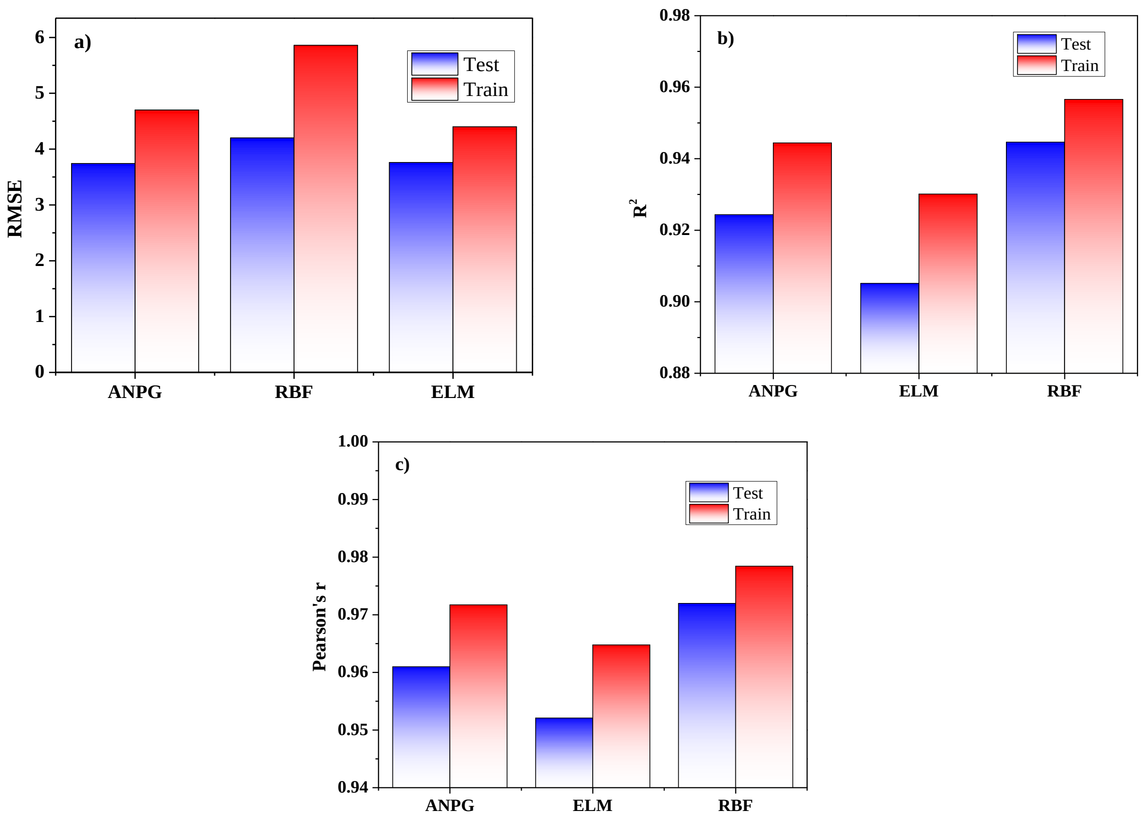

Figure 18. The comparison between the results of the performed algorithms of slip based on the analytical parameters: (**a**) RMSE; (**b**) R^2; (**c**) r.

The calculated equations from the linear regressions are summarized in Tables 8 and 9 where the most decisive equations for both split-tensile load and slip value output of specific steel-concrete specimens manufactured by angle shear connector are highlighted.

Table 8. The calculated tensile-load regression equation of the implemented models.

Model	Network Result	
	Train Phase	Test Phase
	Regression Equation	Regression Equation
ANPG	y = 1.015x − 1.0466	y = 1.0018x − 0.0942
RBF	y = 0.8965x + 3.5193 *	y = 1.0x − 0.0015 **
ELM	y = 0.9403x + 2.6086	y = 0.8777x − 4.5728

* and ** are the best-achieved equations.

Table 9. The calculated slip value regression equation of the implemented models.

Model	Network Result	
	Train Phase	Test Phase
	Regression Equation	Regression Equation
ANPG	y = 0.9405x − 0.0318 *	y = 0.9916x − 0.2411 **
RBF	y = 0.9491x − 0.1464	y = 1.0094x − 0.2069
ELM	y = 1.0421x − 0.6809	y = 0.802x − 1.624

* and ** are the best-achieved equations.

5. Conclusions

In this study, a comparative AI study was conducted to identify the most susceptible structural characteristics of a composite floor system at elevated temperatures and to predict critical strength factors such as failure load and slip value of shear connectors. The main algorithm was a hybridized ANFIS technique with PSO and a GA called the ANPG method. The RBFN and ELM methods were also employed as subsidiary evaluation methods. In addition, this study utilized data from 584 test results which included width (mm), height (mm), thickness (mm), shear load (kN), temperature stages (°C) and slip value (mm). The major findings are as follows:

- Based on the results for slip value output, the ANPG method provided the best result. In this method, the test and training phase evaluation criteria were R^2 (test) = 0.961, R^2 (train) = 0.952; r (test) = 0.980, r (train) = 0.976; and RMSE (test) = 0.962, RMSE (train) = 1.736. Based on the tolerance charts, the test and training phases both represented suitable compatibility, while envelope curves dramatically maintained the same tolerance. According to the error histograms, the normal distribution shapes confirmed appropriate deviation from the mean value, and slip predictions had the least error value among other predictions.
- In general, the RBFN method is an iteration-based algorithm in which most parts are randomly selected. For tensile-load output, the best result was obtained using the RBFN method with the performance parameters of R^2 (test) = 0.946, R^2 (train) = 0.959; r (test) = 0.973, r (train) = 0.973; and RMSE (test) = 3.949, RMSE (train) = 4.585. Tolerance curves in the load section illustrated the best coverage, and error histograms showed the least value in load prediction.
- The ELM method recorded the most suitable results in training phases for slip and split-tensile load prediction. In addition, the ELM method represented the lowest sensitivity against parameter contractions and performed a stable paradigm. For load, the results were R^2 (test) = 0.906, R^2 (train) = 0.932; r (test) = 0.952, r (train) = 0.965; and RMSE (test) = 4.339, RMSE (train) = 6.030. Furthermore, the slip results were R^2 (test) = 0.923, R^2 (train) = 0.922; r (test) = 0.961, r (train) = 0.960; RMSE (test) = 1.455, RMSE (train) = 2.877.
- For the identification study to determine the most critical factors on the shear-bearing capacity of a composite floor system at elevated temperatures, the ANPG method was performed on two subdata models, where slip and temperature were selected as the most significant parameters on the quality of the shear-bearing capacity. Based on the results, it could also be concluded that by restricting slip, the shear-bearing capacity could be improved at elevated temperatures, and conversely.

Finally, although all three methods (ELM, ANPG and RBFN) resulted in satisfactory prediction results, the ANPG method provided the best slip prediction results and the RBFN method achieved better load prediction results; nevertheless, all the above-mentioned methods are suitable for load and slip prediction.

Author Contributions: Conceptualization, P.M. and M.M.; methodology, S.H. and Z.Z.; software, P.M.; validation, P.M., S.H. and Z.Z.; formal analysis, A.M.E.-S.; investigation, A.M.E.-S. and S.H.; resources, Z.Z.; data curation, A.M.E.-S.; writing—original draft preparation, P.M.; writing—review and editing, M.M. and P.M.; visualization, A.M.E.-S.; supervision, M.M.; project administration, P.M.; funding acquisition, M.M. and A.M.E.-S. All authors have read and agreed to the published version of the manuscript.

Funding: This research was funded by Doctoral fund project of Changzhou Vocational Institute of Technology under Grant BS202213101007.

Data Availability Statement: Not applicable.

Acknowledgments: All of the authors like to appreciate the Centre for Infrastructure Engineering of Western Sydney University for all of the technical supports during investigations. The authors extend their appreciation to King Saud University, Saudi Arabia, for funding this work through Researchers Supporting Project number (RSP2023R133), King Saud University, Riyadh, Saudi Arabia.

Conflicts of Interest: The authors declare no conflict of interest.

Appendix A

Table A1. Description of the dataset for analysis.

No.	Temp. (°C)	Height (mm)	Length (mm)	Thick. (mm)	Slip (mm)	Load (kN)	No.	Temp. (°C)	Height (mm)	Length (mm)	Thick. (mm)	Slip (mm)	Load (kN)	No.	Temp. (°C)	Height (mm)	Length (mm)	Thick. (mm)	Slip (mm)	Load (kN)
1	25	65	500	5	0.000	0.000	**31**	550	65	50	5	0.677	33.071	**61**	700	65	50	5	7.641	41.313
2	25	65	50	5	0.021	0.642	**32**	550	65	50	5	0.846	42.382	**62**	700	65	50	5	8.303	40.356
3	25	65	50	5	0.063	5.458	**33**	550	65	50	5	0.972	51.051	**63**	700	65	50	5	8.838	39.236
4	25	65	50	5	0.084	8.508	**34**	550	65	50	5	1.077	57.794	**64**	850	65	50	5	0.000	0.000
5	25	65	50	5	0.083	13.805	**35**	550	65	50	5	1.332	67.266	**65**	850	65	50	5	0.235	0.483
6	25	65	50	5	0.124	17.818	**36**	550	65	50	5	1.524	69.996	**66**	850	65	50	5	0.406	1.287
7	25	65	50	5	0.166	24.881	**37**	550	65	50	5	1.758	70.801	**67**	850	65	50	5	0.598	2.252
8	25	65	50	5	0.165	27.610	**38**	550	65	50	5	2.015	70.321	**68**	850	65	50	5	0.918	3.539
9	25	65	50	5	0.164	30.338	**39**	550	65	50	5	2.293	68.879	**69**	850	65	50	5	1.174	4.825
10	25	65	50	5	0.227	35.957	**40**	550	65	50	5	2.871	65.673	**70**	850	65	50	5	1.664	10.447
11	25	65	50	5	0.290	44.946	**41**	550	65	50	5	3.277	64.232	**71**	850	65	50	5	1.984	14.302
12	25	65	50	5	0.309	55.380	**42**	550	65	50	5	3.961	61.990	**72**	850	65	50	5	2.304	18.478
13	25	65	50	5	0.349	64.529	**43**	550	65	50	5	4.538	60.550	**73**	850	65	50	5	2.453	18.960
14	25	65	50	5	0.432	79.939	**44**	550	65	50	5	5.201	58.950	**74**	850	65	50	5	2.965	23.940
15	25	65	50	5	0.473	85.237	**45**	550	65	50	5	6.163	57.032	**75**	850	65	50	5	3.583	29.563
16	25	65	50	5	0.558	88.287	**46**	550	65	50	5	7.831	52.711	**76**	850	65	50	5	3.882	31.492
17	25	65	50	5	0.708	86.041	**47**	550	65	50	5	8.451	50.630	**77**	850	65	50	5	4.202	33.581
18	25	65	50	5	0.902	80.906	**48**	700	65	50	5	0.000	0.000	**78**	850	65	50	5	4.672	36.474
19	25	65	50	5	1.180	76.254	**49**	700	65	50	5	0.149	1.767	**79**	850	65	50	5	5.099	38.083
20	25	65	50	5	1.694	70.479	**50**	700	65	50	5	0.362	5.621	**80**	850	65	50	5	5.590	39.050
21	25	65	50	5	2.337	65.187	**51**	700	65	50	5	0.724	11.242	**81**	850	65	50	5	6.402	39.377
22	25	65	50	5	2.615	62.942	**52**	700	65	50	5	0.916	15.417	**82**	850	65	50	5	7.770	38.104
23	25	65	50	5	2.829	60.215	**53**	700	65	50	5	1.171	20.876	**83**	850	65	50	5	9.030	37.312
24	25	65	50	5	3.107	58.291	**54**	700	65	50	5	1.852	33.402	**84**	850	65	50	5	10.398	36.520
25	550	65	50	5	0.000	0.000	**55**	700	65	50	5	2.427	43.037	**85**	850	65	50	5	11.317	35.725
26	550	65	50	5	0.042	1.124	**56**	700	65	50	5	3.088	46.253	**86**	850	65	50	5	12.236	35.251
27	550	65	50	5	0.127	5.458	**57**	700	65	50	5	3.815	46.580	**87**	850	65	50	5	13.134	34.937
28	550	65	50	5	0.254	12.522	**58**	700	65	50	5	4.755	46.266	**88**	850	65	50	5	13.732	34.621
29	550	65	50	5	0.359	19.104	**59**	700	65	50	5	6.016	44.671	**89**	850	65	50	5	14.501	34.145
30	550	65	50	5	0.486	25.205	**60**	700	65	50	5	7.064	42.432	**90**	850	65	50	5	15.164	33.830
91	850	65	50	5	15.912	33.354	**126**	550	65	30	5	1.538	27.722	**161**	850	65	30	5	0.818	0.142
92	850	65	50	5	16.296	33.357	**127**	550	65	30	5	1.993	35.697	**162**	850	65	30	5	1.318	0.564
93	850	65	50	5	16.766	33.521	**128**	550	65	30	5	2.447	43.367	**163**	850	65	30	5	2.050	0.946
94	850	65	50	5	17.108	33.364	**129**	550	65	30	5	2.793	49.276	**164**	850	65	30	5	2.718	1.509
95	850	65	50	5	17.215	32.401	**130**	550	65	30	5	3.173	56.738	**165**	850	65	30	5	5.007	5.747
96	25	65	30	5	0.000	0.000	**131**	550	65	30	5	3.164	57.952	**166**	850	65	30	5	6.560	8.699
97	25	65	30	5	0.021	0.038	**132**	550	65	30	5	2.983	56.900	**167**	850	65	30	5	8.215	11.972

Table A1. *Cont.*

No.	Temp. (°C)	Height (mm)	Length (mm)	Thick. (mm)	Slip (mm)	Load (kN)	No.	Temp. (°C)	Height (mm)	Length (mm)	Thick. (mm)	Slip (mm)	Load (kN)	No.	Temp. (°C)	Height (mm)	Length (mm)	Thick. (mm)	Slip (mm)	Load (kN)
98	25	65	30	5	0.059	3.441	**133**	550	65	30	5	2.695	54.393	**168**	850	65	30	5	8.519	12.033
99	25	65	30	5	0.078	5.827	**134**	550	65	30	5	2.320	50.752	**169**	850	65	30	5	10.624	15.568
100	25	65	30	5	0.073	11.160	**135**	550	65	30	5	1.528	42.980	**170**	850	65	30	5	13.042	19.445
101	25	65	30	5	0.113	13.831	**136**	550	65	30	5	1.025	38.327	**171**	850	65	30	5	13.958	20.530
102	25	65	30	5	0.149	19.572	**137**	550	65	30	5	0.190	30.676	**172**	850	65	30	5	14.946	21.715
103	25	65	30	5	0.147	22.320	**138**	550	65	30	5	0.483	24.673	**173**	850	65	30	5	16.341	23.282
104	25	65	30	5	0.145	25.067	**139**	550	65	30	5	1.253	17.834	**174**	850	65	30	5	17.283	23.685
105	25	65	30	5	0.204	28.670	**140**	550	65	30	5	2.344	8.311	**175**	850	65	30	5	18.083	23.265
106	25	65	30	5	0.260	35.666	**141**	550	65	30	5	4.300	9.192	**176**	850	65	30	5	19.000	21.300
107	25	65	30	5	0.272	45.486	**142**	550	65	30	5	5.060	16.176	**177**	850	65	30	5	19.961	16.165
108	25	65	30	5	0.307	53.328	**143**	700	65	30	5	0.000	0.000	**178**	850	65	30	5	20.968	11.812
109	25	65	30	5	0.379	66.104	**144**	700	65	30	5	0.384	1.869	**179**	850	65	30	5	22.082	7.158
110	25	65	30	5	0.417	70.068	**145**	700	65	30	5	1.108	5.870	**180**	850	65	30	5	22.747	3.768
111	25	65	30	5	0.500	70.400	**146**	700	65	30	5	2.217	11.739	**181**	850	65	30	5	23.514	0.699
112	25	65	30	5	0.652	63.344	**147**	700	65	30	5	2.963	16.046	**182**	850	65	30	5	24.311	2.149
113	25	65	30	5	0.848	52.011	**148**	700	65	30	5	3.943	21.680	**183**	850	65	30	5	24.808	4.155
114	25	65	30	5	1.130	38.423	**149**	700	65	30	5	6.287	34.674	**184**	850	65	30	5	25.426	6.803
115	25	65	30	5	1.648	16.172	**150**	700	65	30	5	8.141	44.704	**185**	850	65	30	5	25.987	8.989
116	25	65	30	5	2.294	9.703	**151**	700	65	30	5	9.230	48.374	**186**	850	65	30	5	26.583	11.577
117	25	65	30	5	2.573	2.867	**152**	700	65	30	5	10.000	49.200	**187**	850	65	30	5	26.968	12.660
118	25	65	30	5	2.789	0.461	**153**	700	65	30	5	10.899	49.532	**188**	850	65	30	5	27.491	13.822
119	25	65	30	5	3.069	0.413	**154**	700	65	30	5	11.948	48.804	**189**	850	65	30	5	27.783	14.946
120	550	65	30	5	0.000	0.000	**155**	700	65	30	5	12.698	47.284	**190**	850	65	30	5	27.582	16.210
121	550	65	30	5	0.033	0.788	**156**	700	65	30	5	13.127	46.562	**191**	25	75	30	6	0.000	0.000
122	550	65	30	5	0.239	4.454	**157**	700	65	30	5	13.662	46.059	**192**	25	75	30	6	0.019	0.040
123	550	65	30	5	0.585	10.516	**158**	700	65	30	5	14.048	45.307	**193**	25	75	30	6	0.054	3.636
124	550	65	30	5	0.920	16.265	**159**	850	65	30	5	0.000	0.000	**194**	25	75	30	6	0.071	6.158
125	550	65	30	5	1.202	21.362	**160**	850	65	30	5	0.390	0.180	**195**	25	75	30	6	0.067	11.794
196	25	75	30	6	0.103	14.616	**231**	550	75	30	6	0.937	40.504	**266**	850	75	30	6	12.757	21.696
197	25	75	30	6	0.136	20.684	**232**	550	75	30	6	0.174	32.419	**267**	850	75	30	6	13.661	22.948
198	25	75	30	6	0.134	23.588	**233**	550	75	30	6	0.442	26.074	**268**	850	75	30	6	14.936	24.605
199	25	75	30	6	0.132	26.491	**234**	550	75	30	6	1.145	18.847	**269**	850	75	30	6	15.796	25.031
200	25	75	30	6	0.186	30.298	**235**	550	75	30	6	2.142	8.783	**270**	850	75	30	6	16.528	24.587
201	25	75	30	6	0.238	37.691	**236**	550	75	30	6	3.931	9.715	**271**	850	75	30	6	17.366	22.510
202	25	75	30	6	0.249	48.069	**237**	550	75	30	6	4.625	17.095	**272**	850	75	30	6	18.244	17.083
203	25	75	30	6	0.281	56.357	**238**	700	75	30	6	0.000	0.000	**273**	850	75	30	6	19.165	12.483
204	25	75	30	6	0.346	69.859	**239**	700	75	30	6	0.351	1.976	**274**	850	75	30	6	20.183	7.565
205	25	75	30	6	0.381	74.048	**240**	700	75	30	6	1.013	6.203	**275**	850	75	30	6	20.791	3.982
206	25	75	30	6	0.457	74.399	**241**	700	75	30	6	2.026	12.406	**276**	850	75	30	6	21.492	0.739

Table A1. *Cont.*

No.	Temp. (°C)	Height (mm)	Length (mm)	Thick. (mm)	Slip (mm)	Load (kN)	No.	Temp. (°C)	Height (mm)	Length (mm)	Thick. (mm)	Slip (mm)	Load (kN)	No.	Temp. (°C)	Height (mm)	Length (mm)	Thick. (mm)	Slip (mm)	Load (kN)
207	25	75	30	6	0.595	66.942	**242**	700	75	30	6	2.708	16.957	**277**	850	75	30	6	22.220	2.271
208	25	75	30	6	0.775	54.965	**243**	700	75	30	6	3.604	22.912	**278**	850	75	30	6	22.675	4.391
209	25	75	30	6	1.033	40.605	**244**	700	75	30	6	5.746	36.643	**279**	850	75	30	6	23.239	7.189
210	25	75	30	6	1.506	17.090	**245**	700	75	30	6	7.441	47.243	**280**	850	75	30	6	23.752	9.499
211	25	75	30	6	2.096	10.254	**246**	700	75	30	6	8.436	51.122	**281**	850	75	30	6	24.297	12.234
212	25	75	30	6	2.352	3.029	**247**	700	75	30	6	9.140	51.995	**282**	850	75	30	6	24.649	13.379
213	25	75	30	6	2.550	0.487	**248**	700	75	30	6	9.961	52.346	**283**	850	75	30	6	25.127	14.608
214	25	75	30	6	2.805	0.436	**249**	700	75	30	6	10.920	51.576	**284**	850	75	30	6	25.393	15.795
215	550	75	30	6	0.000	0.000	**250**	700	75	30	6	11.606	49.970	**285**	850	75	30	6	25.210	17.131
216	550	75	30	6	0.030	0.833	**251**	700	75	30	6	11.998	49.206	**286**	25	75	50	6	0.000	0.000
217	550	75	30	6	0.218	4.707	**252**	700	75	30	6	12.487	48.675	**287**	25	75	50	6	0.017	0.708
218	550	75	30	6	0.535	11.114	**253**	700	75	30	6	12.840	47.880	**288**	25	75	50	6	0.051	6.015
219	550	75	30	6	0.841	17.189	**254**	850	75	30	6	0.000	0.000	**289**	25	75	50	6	0.068	9.376
220	550	75	30	6	1.099	22.575	**255**	850	75	30	6	0.356	0.190	**290**	25	75	50	6	0.067	15.213
221	550	75	30	6	1.406	29.296	**256**	850	75	30	6	0.747	0.150	**291**	25	75	50	6	0.101	19.635
222	550	75	30	6	1.821	37.725	**257**	850	75	30	6	1.205	0.596	**292**	25	75	50	6	0.134	27.419
223	550	75	30	6	2.237	45.830	**258**	850	75	30	6	1.874	1.000	**293**	25	75	50	6	0.134	30.426
224	550	75	30	6	2.553	52.075	**259**	850	75	30	6	2.484	1.595	**294**	25	75	50	6	0.134	33.433
225	550	75	30	6	2.900	59.960	**260**	850	75	30	6	4.576	6.073	**295**	25	75	50	6	0.185	39.625
226	550	75	30	6	2.892	61.244	**261**	850	75	30	6	5.996	9.193	**296**	25	75	50	6	0.235	49.531
227	550	75	30	6	2.727	60.132	**262**	850	75	30	6	7.509	12.652	**297**	25	75	50	6	0.251	61.028
228	550	75	30	6	2.463	57.482	**263**	850	75	30	6	7.787	12.717	**298**	25	75	50	6	0.284	71.111
229	550	75	30	6	2.120	53.635	**264**	850	75	30	6	9.711	16.452	**299**	25	75	50	6	0.350	88.093
230	550	75	30	6	1.396	45.421	**265**	850	75	30	6	11.920	20.549	**300**	25	75	50	6	0.384	93.931
301	25	75	50	6	0.453	97.292	**336**	700	75	50	6	0.588	12.388	**371**	850	75	50	6	9.936	38.846
302	25	75	50	6	0.575	94.817	**337**	700	75	50	6	0.743	16.989	**372**	850	75	50	6	10.664	38.500
303	25	75	50	6	0.732	89.159	**338**	700	75	50	6	0.951	23.006	**373**	850	75	50	6	11.150	38.152
304	25	75	50	6	0.958	84.031	**339**	700	75	50	6	1.504	36.809	**374**	850	75	50	6	11.775	37.628
305	25	75	50	6	1.376	77.668	**340**	700	75	50	6	1.970	47.427	**375**	850	75	50	6	12.313	37.280
306	25	75	50	6	1.897	71.836	**341**	700	75	50	6	2.508	50.970	**376**	850	75	50	6	12.920	36.756
307	25	75	50	6	2.123	69.362	**342**	700	75	50	6	3.098	51.331	**377**	850	75	50	6	13.233	36.760
308	25	75	50	6	2.297	66.357	**343**	700	75	50	6	3.861	50.985	**378**	850	75	50	6	13.614	36.941
309	25	75	50	6	2.523	64.237	**344**	700	75	50	6	4.885	49.228	**379**	850	75	50	6	13.892	36.767
310	550	75	50	6	0.000	0.000	**345**	700	75	50	6	5.736	46.760	**380**	850	75	50	6	13.979	35.706
311	550	75	50	6	0.035	1.239	**346**	700	75	50	6	6.204	45.527	**381**	25	100	30	7	0.000	0.000
312	550	75	50	6	0.103	6.015	**347**	700	75	50	6	6.742	44.472	**382**	25	100	30	7	0.171	4.947
313	550	75	50	6	0.206	13.799	**348**	700	75	50	6	7.176	43.238	**383**	25	100	30	7	0.512	11.484
314	550	75	50	6	0.292	21.053	**349**	850	75	50	6	0.000	0.000	**384**	25	100	30	7	0.938	19.611
315	550	75	50	6	0.395	27.775	**350**	850	75	50	6	0.191	0.533	**385**	25	100	30	7	1.279	36.749
316	550	75	50	6	0.549	36.444	**351**	850	75	50	6	0.329	1.419	**386**	25	100	30	7	1.791	47.703

Table A1. *Cont.*

No.	Temp. (°C)	Height (mm)	Length (mm)	Thick. (mm)	Slip (mm)	Load (kN)	No.	Temp. (°C)	Height (mm)	Length (mm)	Thick. (mm)	Slip (mm)	Load (kN)	No.	Temp. (°C)	Height (mm)	Length (mm)	Thick. (mm)	Slip (mm)	Load (kN)
317	550	75	50	6	0.687	46.705	**352**	850	75	50	6	0.485	2.482	**387**	25	100	30	7	2.217	55.654
318	550	75	50	6	0.789	56.258	**353**	850	75	50	6	0.745	3.900	**388**	25	100	30	7	2.900	69.081
319	550	75	50	6	0.875	63.689	**354**	850	75	50	6	0.953	5.317	**389**	25	100	30	7	3.326	75.972
320	550	75	50	6	1.081	74.127	**355**	850	75	50	6	1.352	11.512	**390**	25	100	30	7	3.753	82.156
321	550	75	50	6	1.237	77.136	**356**	850	75	50	6	1.611	15.760	**391**	25	100	30	7	4.606	86.042
322	550	75	50	6	1.428	78.022	**357**	850	75	50	6	1.871	20.362	**392**	25	100	30	7	5.203	86.749
323	550	75	50	6	1.636	77.494	**358**	850	75	50	6	1.992	20.894	**393**	25	100	30	7	5.885	83.569
324	550	75	50	6	1.862	75.904	**359**	850	75	50	6	2.408	26.382	**394**	25	100	30	7	7.249	72.792
325	550	75	50	6	2.331	72.372	**360**	850	75	50	6	2.910	32.579	**395**	25	100	30	7	7.164	66.431
326	550	75	50	6	2.661	70.783	**361**	850	75	50	6	3.152	34.704	**396**	25	100	30	7	7.079	57.244
327	550	75	50	6	3.216	68.313	**362**	850	75	50	6	3.412	37.006	**397**	25	100	30	7	7.164	56.007
328	550	75	50	6	3.685	66.726	**363**	850	75	50	6	3.793	40.194	**398**	550	100	30	7	0.000	0.000
329	550	75	50	6	4.223	64.963	**364**	850	75	50	6	4.140	41.967	**399**	550	100	30	7	0.171	1.060
330	550	75	50	6	5.004	62.849	**365**	850	75	50	6	4.539	43.033	**400**	550	100	30	7	0.597	5.830
331	550	75	50	6	6.358	58.088	**366**	850	75	50	6	5.198	43.394	**401**	550	100	30	7	1.023	13.428
332	550	75	50	6	6.862	55.794	**367**	850	75	50	6	6.309	41.991	**402**	550	100	30	7	1.365	20.318
333	700	75	50	6	0.000	0.000	**368**	850	75	50	6	7.333	41.117	**403**	550	100	30	7	2.047	29.859
334	700	75	50	6	0.121	1.947	**369**	850	75	50	6	8.443	40.245	**404**	550	100	30	7	2.388	37.633
335	700	75	50	6	0.294	6.194	**370**	850	75	50	6	9.190	39.369	**405**	550	100	30	7	3.241	49.117
406	550	100	30	7	4.606	58.834	**441**	700	100	30	7	16.461	34.452	**476**	850	100	30	7	63.642	30.052
407	550	100	30	7	6.482	67.138	**442**	700	100	30	7	17.058	32.862	**477**	850	100	30	7	64.665	29.524
408	550	100	30	7	7.761	70.848	**443**	700	100	30	7	18.081	30.035	**478**	850	100	30	7	66.198	29.704
409	550	100	30	7	8.102	71.378	**444**	850	100	30	7	0.000	0.000	**479**	850	100	30	7	66.880	29.175
410	550	100	30	7	8.870	69.965	**445**	850	100	30	7	0.511	0.886	**480**	850	100	30	7	67.732	29.530
411	550	100	30	7	9.126	63.428	**446**	850	100	30	7	1.874	3.544	**481**	850	100	30	7	70.288	29.005
412	550	100	30	7	9.126	59.187	**447**	850	100	30	7	3.408	6.910	**482**	850	100	30	7	73.695	27.774
413	550	100	30	7	9.126	53.534	**448**	850	100	30	7	4.601	8.506	**483**	25	100	50	7	0.000	0.000
414	550	100	30	7	9.126	48.410	**449**	850	100	30	7	5.708	9.570	**484**	25	100	50	7	0.012	6.257
415	550	100	30	7	9.126	45.936	**450**	850	100	30	7	6.986	11.874	**485**	25	100	50	7	0.088	15.414
416	550	100	30	7	9.126	43.110	**451**	850	100	30	7	8.775	14.887	**486**	25	100	50	7	0.214	26.816
417	550	100	30	7	9.126	39.576	**452**	850	100	30	7	10.650	17.900	**487**	25	100	50	7	0.077	46.573
418	550	100	30	7	9.126	36.749	**453**	850	100	30	7	12.439	20.736	**488**	25	100	50	7	0.030	61.457
419	700	100	30	7	0.000	0.000	**454**	850	100	30	7	14.228	22.863	**489**	25	100	50	7	0.163	72.682
420	700	100	30	7	0.171	1.237	**455**	850	100	30	7	15.676	24.813	**490**	25	100	50	7	0.349	91.349
421	700	100	30	7	0.768	5.124	**456**	850	100	30	7	17.039	25.347	**491**	25	100	50	7	0.522	101.514
422	700	100	30	7	1.365	7.420	**457**	850	100	30	7	18.062	27.297	**492**	25	100	50	7	0.720	110.973
423	700	100	30	7	2.303	15.724	**458**	850	100	30	7	20.021	29.602	**493**	25	100	50	7	1.429	121.409
424	700	100	30	7	3.156	24.205	**459**	850	100	30	7	22.066	30.845	**494**	25	100	50	7	2.000	126.700
425	700	100	30	7	3.923	32.156	**460**	850	100	30	7	23.855	32.088	**495**	25	100	50	7	2.800	128.759
426	700	100	30	7	4.947	40.106	**461**	850	100	30	7	27.348	34.220	**496**	25	100	50	7	4.562	128.461

Table A1. *Cont.*

No.	Temp. (°C)	Height (mm)	Length (mm)	Thick. (mm)	Slip (mm)	Load (kN)	No.	Temp. (°C)	Height (mm)	Length (mm)	Thick. (mm)	Slip (mm)	Load (kN)	No.	Temp. (°C)	Height (mm)	Length (mm)	Thick. (mm)	Slip (mm)	Load (kN)
427	700	100	30	7	5.714	45.583	**462**	850	100	30	7	27.774	33.867	**497**	25	100	50	7	4.712	121.445
428	700	100	30	7	6.482	50.000	**463**	850	100	30	7	33.568	36.358	**498**	25	100	50	7	4.966	111.603
429	700	100	30	7	7.676	55.654	**464**	850	100	30	7	34.420	35.474	**499**	25	100	50	7	5.097	111.021
430	700	100	30	7	8.955	60.071	**465**	850	100	30	7	35.612	36.716	**500**	550	100	50	7	0.000	0.000
431	700	100	30	7	10.576	62.544	**466**	850	100	30	7	36.976	35.834	**501**	550	100	50	7	0.131	1.783
432	700	100	30	7	12.111	63.251	**467**	850	100	30	7	41.576	37.260	**502**	550	100	50	7	0.382	8.359
433	700	100	30	7	12.623	61.307	**468**	850	100	30	7	43.280	37.972	**503**	550	100	50	7	0.528	17.763
434	700	100	30	7	13.646	56.360	**469**	850	100	30	7	46.603	39.041	**504**	550	100	50	7	0.615	26.099
435	700	100	30	7	13.902	54.240	**470**	850	100	30	7	47.199	38.689	**505**	550	100	50	7	0.945	38.529
436	700	100	30	7	14.328	50.353	**471**	850	100	30	7	51.118	39.405	**506**	550	100	50	7	0.999	47.748
437	700	100	30	7	15.437	45.583	**472**	850	100	30	7	53.419	39.056	**507**	550	100	50	7	1.428	62.845
438	700	100	30	7	15.693	43.463	**473**	850	100	30	7	55.804	39.416	**508**	550	100	50	7	2.434	78.343
439	700	100	30	7	15.778	40.636	**474**	850	100	30	7	58.956	37.830	**509**	550	100	50	7	4.003	94.595
440	700	100	30	7	15.864	37.633	**475**	850	100	30	7	61.086	36.949	**510**	550	100	50	7	5.146	103.725
511	550	100	50	7	5.467	105.700	**536**	700	100	50	7	11.320	92.359	**561**	850	100	50	7	8.301	38.313
512	550	100	50	7	6.287	107.538	**537**	700	100	50	7	11.663	90.914	**562**	850	100	50	7	7.735	40.161
513	550	100	50	7	6.784	102.085	**538**	700	100	50	7	12.250	88.152	**563**	850	100	50	7	6.341	43.475
514	550	100	50	7	6.941	97.845	**539**	700	100	50	7	13.556	86.307	**564**	850	100	50	7	5.567	43.266
515	550	100	50	7	7.149	92.191	**540**	700	100	50	7	13.899	84.862	**565**	850	100	50	7	2.226	47.717
516	550	100	50	7	7.339	87.067	**541**	700	100	50	7	14.101	82.260	**566**	850	100	50	7	0.504	47.122
517	550	100	50	7	7.430	84.594	**542**	700	100	50	7	14.310	79.481	**567**	850	100	50	7	0.534	48.768
518	550	100	50	7	7.534	81.767	**543**	700	100	50	7	15.038	77.876	**568**	850	100	50	7	1.697	48.347
519	550	100	50	7	7.665	78.233	**544**	700	100	50	7	15.701	77.861	**569**	850	100	50	7	4.894	51.330
520	550	100	50	7	7.769	75.406	**545**	700	100	50	7	16.841	77.734	**570**	850	100	50	7	5.897	52.618
521	700	100	50	7	0.000	0.000	**546**	850	100	50	7	0.000	0.000	**571**	850	100	50	7	8.167	54.812
522	700	100	50	7	0.120	1.687	**547**	850	100	50	7	0.361	1.059	**572**	850	100	50	7	9.111	54.661
523	700	100	50	7	0.556	7.149	**548**	850	100	50	7	1.615	4.178	**573**	850	100	50	7	12.324	56.704
524	700	100	50	7	1.058	11.020	**549**	850	100	50	7	3.395	8.063	**574**	850	100	50	7	14.968	57.133
525	700	100	50	7	1.654	21.799	**550**	850	100	50	7	3.773	10.063	**575**	850	100	50	7	17.000	58.300
526	700	100	50	7	2.157	32.530	**551**	850	100	50	7	3.713	11.502	**576**	850	100	50	7	21.714	57.781
527	700	100	50	7	2.596	42.505	**552**	850	100	50	7	4.704	14.238	**577**	850	100	50	7	24.710	57.621
528	700	100	50	7	3.291	53.156	**553**	850	100	50	7	5.880	17.856	**578**	850	100	50	7	34.056	51.589
529	700	100	50	7	3.833	60.658	**554**	850	100	50	7	6.972	21.504	**579**	850	100	50	7	35.599	51.407
530	700	100	50	7	4.418	67.099	**555**	850	100	50	7	7.975	24.945	**580**	850	100	50	7	36.955	52.106
531	700	100	50	7	5.379	75.903	**556**	850	100	50	7	8.281	27.678	**581**	850	100	50	7	38.158	51.807
532	700	100	50	7	6.476	83.695	**557**	850	100	50	7	8.752	30.118	**582**	850	100	50	7	38.659	52.451
533	700	100	50	7	7.994	90.443	**558**	850	100	50	7	7.915	31.114	**583**	850	100	50	7	41.732	52.791
534	700	100	50	7	9.500	95.200	**559**	850	100	50	7	8.811	33.409	**584**	850	100	50	7	46.353	52.713
535	700	100	50	7	10.092	94.606	**560**	850	100	50	7	9.121	36.377							

References

1. Utsab Katwal, T.A.; Tao, Z.; Uy, B.; Rahme, D. Tests of circular geopolymer concrete-filled steel columns under ambient and fire conditions. *J. Constr. Steel Res.* **2022**, *196*, 107393. [CrossRef]
2. Xia, Y.; Shi, M.; Zhang, C.; Wang, C.; Sang, X.; Liu, R.; Zhao, P.; An, G.; Fang, H. Analysis of flexural failure mechanism of ultraviolet cured-in-place-pipe materials for buried pipelines rehabilitation based on curing temperature monitoring. *Eng. Fail. Anal.* **2022**, *142*, 106763. [CrossRef]
3. Liu, K.; Yang, Z.; Wei, W.; Gao, B.; Xin, D.; Sun, C.; Gao, G.; Wu, G. Novel Detection Approach for Thermal Defects: Study on Its Feasibility and Application to Vehicle Cables. *High Volt.* **2022**. [CrossRef]
4. Huang, H.; Yao, Y.; Liang, C.; Ye, Y. Experimental study on cyclic performance of steel-hollow core partially encased composite spliced frame beam. *Soil Dyn. Earthq. Eng.* **2022**, *163*, 107499. [CrossRef]
5. Zhang, Z.; Yang, Q.; Yu, Z.; Wang, H.; Zhang, T. Influence of Y2O3 addition on the microstructure of TiC reinforced Ti-based composite coating prepared by laser cladding. *Mater. Charact.* **2022**, *189*, 111962. [CrossRef]
6. Zhang, C.; Abedini, M. Development of PI model for FRP composite retrofitted RC columns subjected to high strain rate loads using LBE function. *Eng. Struct.* **2022**, *252*, 113580. [CrossRef]
7. Zhao, G.; Shi, L.; Yang, G.; Zhuang, X.; Cheng, B. 3D fibrous aerogels from 1D polymer nanofibers for energy and environmental applications. *J. Mater. Chem. A* **2023**. [CrossRef]
8. Li, J.; Chen, M.; Li, Z. Improved soil–structure interaction model considering time-lag effect. *Comput. Geotech.* **2022**, *148*, 104835. [CrossRef]
9. Deng, E.-F.; Zhang, Z.; Zhang, C.-X.; Tang, Y.; Wang, W.; Du, Z.-J.; Gao, J.-P. Experimental study on flexural behavior of UHPC wet joint in prefabricated multi-girder bridge. *Eng. Struct.* **2023**, *275*, 115314. [CrossRef]
10. Tian, L.-m.; Li, M.-h.; Li, L.; Li, D.-y.; Bai, C. Novel joint for improving the collapse resistance of steel frame structures in column-loss scenarios. *Thin-Walled Struct.* **2023**, *182*, 110219. [CrossRef]
11. AzariJafari, H.; Amiri, M.J.T.; Ashrafian, A.; Rasekh, H.; Barforooshi, M.J.; Berenjian, J. Ternary blended cement: An eco-friendly alternative to improve resistivity of high-performance self-consolidating concrete against elevated temperature. *J. Clean. Prod.* **2019**, *223*, 575–586. [CrossRef]
12. Toghroli, A.; Mehrabi, P.; Shariati, M.; Trung, N.T.; Jahandari, S.; Rasekh, H. Evaluating the use of recycled concrete aggregate and pozzolanic additives in fiber-reinforced pervious concrete with industrial and recycled fibers. *Constr. Build. Mater.* **2020**, *252*, 118997. [CrossRef]
13. Rahai, A.; Mortazavi, M. Experimental and numerical study on the effect of core shape and concrete cover length on the behavior of BRBs. *Int. J. Civ. Eng.* **2014**, *12*, 379–395.
14. Mehrabi, P.; Shariati, M.; Kabirifar, K.; Jarrah, M.; Rasekh, H.; Trung, N.T.; Shariati, A.; Jahandari, S. Effect of pumice powder and nano-clay on the strength and permeability of fiber-reinforced pervious concrete incorporating recycled concrete aggregate. *Constr. Build. Mater.* **2021**, *287*, 122652. [CrossRef]
15. Ren, C.; Yu, J.; Liu, S.; Yao, W.; Zhu, Y.; Liu, X. A plastic strain-induced damage model of porous rock suitable for different stress paths. *Rock Mech. Rock Eng.* **2022**, *55*, 1887–1906. [CrossRef]
16. Hussain, I.; Yaqub, M.; Mortazavi, M.; Ehsan, M.A.; Uzair, M. Finite Element Modeling and Statistical Analysis of Fire-Damaged Reinforced Concrete Columns Repaired Using Smart Materials and FRP Confinement. In Proceedings of the International Conference on Fibre-Reinforced Polymer (FRP) Composites in Civil Engineering, Istanbul, Turkey, 8–10 December 2021; Springer: Berlin/Heidelberg, Germany, 2021; pp. 101–110.
17. Shariati, M.; Tahmasbi, F.; Mehrabi, P.; Bahadori, A.; Toghroli, A. Monotonic behavior of C and L shaped angle shear connectors within steel-concrete composite beams: An experimental investigation. *Steel Compos. Struct* **2020**, *35*, 237–247.
18. Shariati, M.; Trung, N.T.; Wakil, K.; Mehrabi, P.; Safa, M.; Khorami, M. Estimation of moment and rotation of steel rack connections using extreme learning machine. *Steel Compos. Struct.* **2019**, *31*, 427–435.
19. Shariati, M.; Mafipour, M.S.; Mehrabi, P.; Bahadori, A.; Zandi, Y.; Salih, M.N.; Nguyen, H.; Dou, J.; Song, X.; Poi-Ngian, S. Application of a hybrid artificial neural network-particle swarm optimization (ANN-PSO) model in behavior prediction of channel shear connectors embedded in normal and high-strength concrete. *Appl. Sci.* **2019**, *9*, 5534. [CrossRef]
20. Pashan, A. *Behaviour of Channel Shear Connectors: Push-Out Tests*; University of Saskatchewan: Saskatoon, SK, Canada, 2006.
21. Sharafi, P.; Mortazavi, M.; Askarian, M.; Uz, M.E.; Zhang, C.; Zhang, J. Thin walled steel sections' free shape optimization using charged system search algorithm. *Iran Univ. Sci. Technol.* **2017**, *7*, 515–526.
22. Lee, J.-S.; Shin, K.-J.; Lee, H.-D.; Woo, J.-H. Strength Evaluation of Angle Type Shear Connectors in Composite Beams. *Int. J. Steel Struct.* **2020**, *20*, 2068–2075. [CrossRef]
23. Davoodnabi, S.M. Behavior of steel-concrete composite beam using angle shear connectors at fire condition. *Steel Compos. Struct. Int. J.* **2019**, *30*, 141–147.
24. Firouzianhaji, A.; Usefi, N.; Samali, B.; Mehrabi, P. Shake table testing of standard cold-formed steel storage rack. *Appl. Sci.* **2021**, *11*, 1821. [CrossRef]
25. Shariati, M.; Faegh, S.S.; Mehrabi, P.; Bahavarnia, S.; Zandi, Y.; Masoom, D.R.; Toghroli, A.; Trung, N.-T.; Salih, M.N. Numerical study on the structural performance of corrugated low yield point steel plate shear walls with circular openings. *Steel Compos. Struct. Int. J.* **2019**, *33*, 569–581.

26. Mehrabi, P.; Honarbari, S.; Rafiei, S.; Jahandari, S.; Alizadeh Bidgoli, M. Seismic response prediction of FRC rectangular columns using intelligent fuzzy-based hybrid metaheuristic techniques. *J. Ambient Intell. Humaniz. Comput.* **2021**, *12*, 10105–10123. [CrossRef]
27. Jahed Armaghani, D.; Hasanipanah, M.; Bakhshandeh Amnieh, H.; Tien Bui, D.; Mehrabi, P.; Khorami, M. Development of a novel hybrid intelligent model for solving engineering problems using GS-GMDH algorithm. *Eng. Comput.* **2020**, *36*, 1379–1391. [CrossRef]
28. Taheri, E.; Firouzianhaji, A.; Mehrabi, P.; Vosough Hosseini, B.; Samali, B. Experimental and numerical investigation of a method for strengthening cold-formed steel profiles in bending. *Appl. Sci.* **2020**, *10*, 3855. [CrossRef]
29. Taheri, E.; Firouzianhaji, A.; Usefi, N.; Mehrabi, P.; Ronagh, H.; Samali, B. Investigation of a method for strengthening perforated cold-formed steel profiles under compression loads. *Appl. Sci.* **2019**, *9*, 5085. [CrossRef]
30. Taheri, E.; Mehrabi, P.; Rafiei, S.; Samali, B. Numerical Evaluation of the Upright Columns with Partial Reinforcement along with the Utilisation of Neural Networks with Combining Feature-Selection Method to Predict the Load and Displacement. *Appl. Sci.* **2021**, *11*, 11056. [CrossRef]
31. Xu, H.; He, T.; Zhong, N.; Zhao, B.; Liu, Z. Transient thermomechanical analysis of micro cylindrical asperity sliding contact of SnSbCu alloy. *Tribol. Int.* **2022**, *167*, 107362. [CrossRef]
32. Xiao, D.; Hu, Y.; Wang, Y.; Deng, H.; Zhang, J.; Tang, B.; Xi, J.; Tang, S.; Li, G. Wellbore cooling and heat energy utilization method for deep shale gas horizontal well drilling. *Appl. Therm. Eng.* **2022**, *213*, 118684. [CrossRef]
33. Li, J.; Zhou, L.; Li, S.; Lin, G.; Ding, Z. Soil–structure interaction analysis of nuclear power plant considering three-dimensional surface topographic irregularities based on automatic octree mesh. *Eng. Struct.* **2023**, *275*, 115161. [CrossRef]
34. Shariati, M.; Mafipour, M.S.; Mehrabi, P.; Shariati, A.; Toghroli, A.; Trung, N.T.; Salih, M.N. A novel approach to predict shear strength of tilted angle connectors using artificial intelligence techniques. *Eng. Comput.* **2021**, *37*, 2089–2109. [CrossRef]
35. Li, J.; Cheng, F.; Lin, G.; Wu, C. Improved hybrid method for the generation of ground motions compatible with the multi-damping design spectra. *J. Earthq. Eng.* **2022**, 1–27. [CrossRef]
36. Huang, Z.; Li, T.; Huang, K.; Ke, H.; Lin, M.; Wang, Q. Predictions of flow and temperature fields in a T-junction based on dynamic mode decomposition and deep learning. *Energy* **2022**, *261*, 125228. [CrossRef]
37. Liu, J.; Mohammadi, M.; Zhan, Y.; Zheng, P.; Rashidi, M.; Mehrabi, P. Utilizing Artificial Intelligence to Predict the Superplasticizer Demand of Self-Consolidating Concrete Incorporating Pumice, Slag, and Fly Ash Powders. *Materials* **2021**, *14*, 6792. [CrossRef]
38. Khotbehsara, M.M.; Miyandehi, B.M.; Naseri, F.; Ozbakkaloglu, T.; Jafari, F.; Mohseni, E. Effect of SnO_2, ZrO_2, and $CaCO_3$ nanoparticles on water transport and durability properties of self-compacting mortar containing fly ash: Experimental observations and ANFIS predictions. *Constr. Build. Mater.* **2018**, *158*, 823–834. [CrossRef]
39. Feng, Y.; Mohammadi, M.; Wang, L.; Rashidi, M.; Mehrabi, P. Application of artificial intelligence to evaluate the fresh properties of self-consolidating concrete. *Materials* **2021**, *14*, 4885. [CrossRef] [PubMed]
40. Huang, Y.; Fu, J. Review on application of artificial intelligence in civil engineering. *Comput. Model. Eng. Sci.* **2019**, *121*, 845–875. [CrossRef]
41. Huang, J.; Ling, S.; Wu, X.; Deng, R. GIS-based comparative study of the bayesian network, decision table, radial basis function network and stochastic gradient descent for the spatial prediction of landslide susceptibility. *Land* **2022**, *11*, 436. [CrossRef]
42. Khambra, G.; Shukla, P. Novel machine learning applications on fly ash based concrete: An overview. *Mater. Today Proc.* **2021**. [CrossRef]
43. Shariati, M.; Mafipour, M.S.; Mehrabi, P.; Zandi, Y.; Dehghani, D.; Bahadori, A.; Shariati, A.; Trung, N.T.; Salih, M.; Poi-Ngian, S. Application of Extreme Learning Machine (ELM) and Genetic Programming (GP) to design steel-concrete composite floor systems at elevated temperatures. *Steel Compos. Struct* **2019**, *33*, 319–332.
44. Walia, N.; Singh, H.; Sharma, A. ANFIS: Adaptive neuro-fuzzy inference system-a survey. *Int. J. Comput. Appl.* **2015**, *123*. [CrossRef]
45. Shahgoli, A.F.; Zandi, Y.; Heirati, A.; Khorami, M.; Mehrabi, P.; Petkovic, D. Optimisation of propylene conversion response by neuro-fuzzy approach. *Int. J. Hydromechatronics* **2020**, *3*, 228–237. [CrossRef]
46. Eberhart, R.; Kennedy, J. Particle swarm optimization. In Proceedings of the IEEE International Conference on Neural Networks, Perth, Australia, 27 November–1 December 1995; IEEE: Piscataway, NJ, USA, 1995; pp. 1942–1948.
47. Holland, J.H. Genetic algorithms. *Sci. Am.* **1992**, *267*, 66–73. [CrossRef]
48. Booker, L.B.; Goldberg, D.E.; Holland, J.H. Classifier systems and genetic algorithms. *Artif. Intell.* **1989**, *40*, 235–282. [CrossRef]
49. Camp, C.V.; Pezeshk, S.; Hansson, H. Flexural design of reinforced concrete frames using a genetic algorithm. *J. Struct. Eng.* **2003**, *129*, 105–115. [CrossRef]
50. Huang, G.-B.; Zhu, Q.-Y.; Siew, C.-K. Extreme learning machine: Theory and applications. *Neurocomputing* **2006**, *70*, 489–501. [CrossRef]
51. Ikram, R.M.A.; Dai, H.-L.; Al-Bahrani, M.; Mamlooki, M. Prediction of the FRP Reinforced Concrete Beam shear capacity by using ELM-CRFOA. *Measurement* **2022**, *205*, 112230. [CrossRef]
52. Zhang, M.; Wang, K.; Zhang, C.; Chen, H.; Liu, H.; Yue, Y.; Luffman, I.; Qi, X. Using the radial basis function network model to assess rocky desertification in northwest Guangxi, China. *Environ. Earth Sci.* **2011**, *62*, 69–76. [CrossRef]

53. Bodyanskiy, Y.; Pirus, A.; Deineko, A. Multilayer radial-basis function network and its learning. In Proceedings of the 2020 IEEE 15th International Conference on Computer Sciences and Information Technologies (CSIT), Zbarazh, Ukraine, 23–26 September 2020; pp. 92–95.
54. Shahmansouri, A.A.; Akbarzadeh Bengar, H.; Ghanbari, S. Experimental investigation and predictive modeling of compressive strength of pozzolanic geopolymer concrete using gene expression programming. *J. Concr. Struct. Mater.* **2020**, *5*, 92–117.
55. Shahmansouri, A.A.; Yazdani, M.; Ghanbari, S.; Bengar, H.A.; Jafari, A.; Ghatte, H.F. Artificial neural network model to predict the compressive strength of eco-friendly geopolymer concrete incorporating silica fume and natural zeolite. *J. Clean. Prod.* **2021**, *279*, 123697. [CrossRef]
56. Shahmansouri, A.A.; Yazdani, M.; Hosseini, M.; Bengar, H.A.; Ghatte, H.F. The prediction analysis of compressive strength and electrical resistivity of environmentally friendly concrete incorporating natural zeolite using artificial neural network. *Constr. Build. Mater.* **2022**, *317*, 125876. [CrossRef]